ÇUKUROVA UNIVERSITY
INSTITUTE OF NATURAL AND APPLIED SCIENCES

MSc THESIS

Arif Emre AKTAŞ

THERMODYNAMIC SIMULATION OF TRANSCRITICAL ORGANIC RANKINE VAPOR COMPRESSION REFRIGERATION SYSTEM USING LOW GWP REFRIGERANTS

DEPARTMENT OF AUTOMOTIVE ENGINEERING

ADANA-2017

ÇUKUROVA UNIVERSITY
INSTITUTE OF NATURAL AND APPLIED SCIENCES

THERMODYNAMIC SIMULATION OF TRANSCRITICAL ORGANIC RANKINE VAPOR COMPRESSION REFRIGERATION SYSTEM USING LOW GWP REFRIGERANTS

Arif Emre AKTAŞ

MSc THESIS

DEPARTMENT OF AUTOMOTIVE ENGINEERING

We certify that the thesis titled above was reviewed and approved for the award of degree of the Master of Science by the board of jury on 24/01/2017

…….	……	……..
Prof. Dr. Alper YILMAZ	Assoc. Prof. Dr. Hasan SERİN	Asst. Prof. Dr. Erinç ULUDAMAR
SUPERVISOR	MEMBER	MEMBER

This MSc Thesis is written at the Department of Institute of Natural and Applied Sciences of Çukurova University.
Registration Number:

Prof. Dr. Mustafa Gök
Director
Institute of Natural and Applied Sciences

ABSTRACT

MSc THESIS

THERMODYNAMIC SIMULATION OF TRANSCRITICAL ORGANIC RANKINE VAPOR COMPRESSION REFRIGERATION SYSTEM USING LOW GWP REFRIGERANTS

ARİF EMRE AKTAŞ

ÇUKUROVA UNIVERSITY
INSTITUTE OF NATURAL AND APPLIED SCIENCES
DEPARTMENT OF AUTOMOTIVE ENGINEERING

Supervisor : Prof. Dr. Alper YILMAZ
: Year: 2017, Pages: 92
Jury : Prof. Dr. Alper YILMAZ
: Assoc. Prof. Dr. Hasan SERİN
: Asst. Prof. Dr. Erinç ULUDAMAR

Due to critical level of greenhouse gas emissions and rising petroleum prices, governments have issued strict regulations for internal combustion engine emissions and fuel economy standarts. Organic Rankine cycle is a promising way to recover engine exhaust waste heat and reduce fuel consumption.

In this thesis, parametric thermodynamic analysis of transcritical organic Rankine vapor compression (T-ORVC) refrigeration cycle using internal combustion engine exhaust waste heat is investigated. Two low Global Warming Potential (GWP) fluids are considered as refrigerants for the potential replacement of high GWP refrigerant R134a.

Throughout the theoretical study, refrigerant boiler pressure, cycle component efficiencies and temperature of condenser/evaporator and the degree of subcooling/superheating are used as parameters to simulate all possible scenarios. Results revealed that both low GWP working fluids have cooling performance close to R134a. Moreover, T-ORVC refrigeration system with R1234ze(E) presented slightly higher thermodynamic performance throughout the operation conditions.

Study indicated that, R134a can be replaced by studied low GWP working fluids for the proposed system.

Key Words: Engine exhaust heat, Air conditioning, Rankine cycle, Vapor compression cycle, Transcritical cycle

ÖZ

YÜKSEK LİSANS TEZİ

GWP ORANI DÜŞÜK AKIŞKANLARIN KULLANILDIĞI TRANSKRİTİK ORGANİK RANKINE ÇEVRİMİNDEN GÜÇ ALAN BUHAR SIKIŞTIRMALI SOĞUTMA SİSTEMİNİN TERMODİNAMİK SİMÜLASYONU

Arif Emre AKTAŞ

ÇUKUROVA ÜNİVERSİTESİ
FEN BİLİMLERİ ENSTİTÜSÜ
OTOMOTİV MÜHENDİSLİĞİ ANABİLİM DALI

Danışman : Prof. Dr. Alper YILMAZ
: Yıl: 2017, Sayfa: 92
Jüri : Prof. Dr. Alper YILMAZ
: Doç. Dr. Hasan SERİN
: Yrd. Doç. Dr. Erinç ULUDAMAR

Kritik seviyedeki sera gazı emisyonları ve yükselen petrol fiyatları nedeniyle ülke yönetimleri içten yanmalı motor emisyonları ve yakıt ekonomi standartları için sıkı düzenlemeler yürürlüğe koymuşlardır. Motor atık ısısı geri kazanımı ve yakıt tüketiminin düşürülmesi için organik Rankine çevrimi umut vericidir.

Bu tezde, içten yanmalı motor atık ısısının kullanıldığı transkritik organik Rankine çevriminden güç alan buhar sıkıştırmalı soğutma sisteminin (T-ORVC) parametrik termodinamik analizi yapılmıştır. Küresel ısınma potansiyeli (GWP) yüksek R134a soğutucu akışkanının yerine kullanılabilecek GWP'si düşük iki akışkan incelenmiştir.

Teorik çalışma boyunca, olası tüm senaryoların simülasyonu için soğutucu akışkan kazan basıncı, çevrim bileşenlerinin verimleri, yoğuşturucu/evaporator sıcaklıkları, aşırı kızdırma/aşırı soğutma dereceleri parametre olarak kullanılmıştır. Çalışma sonuçları her iki iş gören akışkanın R134a'ya yakın performans sergilediğini ortaya koymuştur. Dahası, R1234ze(E)'nin kullanıldığı T-ORVC daha yüksek termodinamik performans sergilemiştir.

Yapılan çalışma, incemesi yapılan akışkanların R134a ile değiştirilebileceğini göstermiştir.

Anahtar Kelimeler: Motor egzoz ısısı, İklimlendirme, Rankine çevrimi, Buhar sıkıştırmalı çevrim, Transkritik çevrim

EXTENDED SUMMARY

Son zamanlarda, atık ısı geri kazanımı fosil yakıtların sınırlı miktarda olması ve bunların tüketilmeleri sonucu çevreye vermiş olduğu zarar nedeniyle daha fazla ilgi çekmektedir. Araştırmacılar Kalina, Goswami, emme (absorpsion adsorpsion) çevrimi organik Rankine çevrimi (ORC) gibi çeşitli ısı geri kazanım çevrimleri üzerinde çalışmışlardır. ORC, 75-525 ^{o}C gibi geniş sıcaklık aralıklarındaki termal enerjiyi bütün bir yıl boyunca kesintisiz olarak kullanabilme esnekliğine sahiptir. ORC, aynı zamanda geniş alanlarda kullanılan bir teknolojidir ve diğer çevrimlere oranla daha yüksek seviyede atık ısının geri kazanımını sağlamaktadır.

Rankine çevrimi için iş gören akışkan CO_2, amonyak, su ve organik bileşikler olabilmektedir. Bunların içerisinde organik akışkanlar düşük dereceli termal enerjinin geri kazanımı için en uygun tercihtir. Bunun yanısıra, diğer akışkanlarla kıyaslandığında organik akışkanlar daha düşük kaynama noktası, daha büyük molekül kütlesi ve daha yüksek kütlesel debiye sahiptir. Bu özellikler, ORC sitemlerinin türbin verimini daha yüksek kılmaktadır.

Mobil iklimlendirme sistemlerinde, 1990'lı yıllarda Montreal protokolü sonrasında ozon tabakasının daha fazla zarar görmemesi için soğutucu akışkan R12'nin yerine R134a kullanılmaya başlanmıştır. R134a, ozon tabakasını inceltme potansiyeli sıfır olan bir akışkan olmasına rağmen, yüksek küresel ısınma potansiyeline (GWP) sahip bir sera gazıdır. Ayrıca troposfer tabakasına ulaşan R134a'nın, yakın gelecekte güneş ışınları ile ayrıştırılıp asitli ve zehirli molekillerin oluşmasına neden olabileceği ifade edilmiştir. Bu durum, geçmişte kloroflorokarbonun (CFC) yapmış olduğu çevresel zarardan daha büyük felaketlere neden olabilir. Kyoto protokolünün yürülülüğe girmesi sonrası, R134a kullanımı sınırlandırılmıştır. Bu nedenle R134a'nın yerine alternatif olarak görülen ve hidrofloroolefin (HFO) sınıfından olan ve sıfır ODP ile birlikte birin altında GWP değerine sahip iki akışkan olan R1234yf ve R1234ze(E) öngörülmektedir.

Bu tezde, içten yanmalı motor atık ısısının kullanıldığı transkritik organik Rankine çevriminden güç alan buhar sıkıştırmalı soğutma sisteminin parametrik termodinamik analizi yapılmıştır. Küresel ısınma potansiyeli (GWP) yüksek R134a soğutucu akışkanının yerine kullanılabilecek GWP'si düşük iki akışkan incelenmiştir.

Öncelikle soğutucu akışkanların tarihsel gelişimi incelenmiştir. Daha sonra akışkanların sınıflandırılması ve seçimindeki kriterlerin neler olduğu ve tarih boyunca nasıl değiştiği ifade edilmiştir. Günümüzde en çok kullanılan soğutucu akışkanların fiziksel ve çevresel özellikleri verilmiştir.

Simülasyonun canlandırılmasında termodinamik sistemler için güçlü bir problem çözücü olan ve birçok araştırmacı tarafından tercih edilen "Engineering Equation Solver (EES)" yazılımı kullanılmıştır. Yazılım içerisinde, kullanılacak akışkanların malzeme özelliklerinden matematiksel fonksiyonlarına kadar her türlü hesaplamayı yapabilecek veriler yüklenmiş durumdadır.

Teorik çalışma boyunca, olası tüm senaryoların simülasyonu için soğutucu akışkan kazan basıncı, çevrim bileşenlerinin verimleri, yoğuşturucu/evaporator sıcaklıkları, aşırı kızdırma/aşırı soğutma dereceleri parametre olarak kullanılmış olup bu parametrelerin performans katsayısına (COP) etkisi incelenmiştir.

Modeli yapılan sistem organik Rankine çevrimi ile mobil sistemlerde en çok kullanılan buhar sıkıştırmalı soğutma çevriminin birleşiminden oluşmaktadır. ORC çevrimine ait türbin ile soğutma çevrimine ait kompresör bir mil yardımı ile birbirlerine doğrudan bağlanmıştır. ORC atık ısıdan elde etmiş olduğu dönme hareketini soğutma çevriminin kompresörüne iletir daha sonra soğutma çevrimi aldığı mekanik enerji soğutma olarak ortama vermektedir. Sistemde her iki çevrim için ortak bir yoğuşturucu kullanılmıştır.

Çalışmada, parametre aralığı olarak 100-200 ºC kazan sıcaklığı, 0-15 ºC yoğuşturucu sıcaklığı, 45-60 ºC evaporatör sıcaklığı, 30, 80 bar kazan basıncı, düşük, orta ve yüksek sistem bileşen verimleri ve 1 ve 5 ºC kritikaltı/kritiküstü

sıcaklık aralıkları ele alınıp bu parametrelerin performans katsayılarına etkileri incelenmiştir.

Sonuçlar, T-ORVC sisteminde iş gören akışkan olarak kullanılan R1234ze(E)'nin analizi yapılan tüm parametreler içinde en yüksek COPT değerini verdiğini göstermiştir. Diğer taraftan R1234yf ise, R134'nın biraz altında COPT değerleri vermiştir. Ayrıca, COP değerlerinin kazan ve evaporator sıcaklıkları, kazan basıncı ve aşırı ısıtma/aşırı soğutma sıcaklık farkları ve sistem bileşenleri verimleri ile arttığı yoğuşturucu sıcaklığı ile azaldığı görülmüştür.

En yüksek COP değerine sahip R1234ze(E)'nin kritik noktanın altındaki basınç değerlerinde diğer akışkanlara oranla daha yüksek COPT değerine sahip olduğu görülmüştür. Kritik altı basınçlar için R1234ze(E) ile R134a'nın COPT farkları yaklaşık olarak %14 ile %33 arasında değişmektedir. Kritiküstü basınçlarda ise bu fark en fazla %4 civarı olmaktadır.

R134a, R1234yf ve R1234ze(E) için 200 ºC kazan sıcaklığında, 80 bar kazan basıncında yüksek bileşen verimleri kullanılarak elde edilen en yüksek COPT değerleri sırasıyla 1.084, 1.015 and 1.127 olmaktadır.

Genel olarak elde edilen COPW değerleri çok yüksektir. Böylece kazan ile karşılaştırıldığında, pompa için gerekli elektrik enerjisi çok düşüktür.

Bu tez çalışması simülasyonu yapılan sistemde her iki düşük GWP'li iş gören akışkanın yüksek GWP değerine sahip R134a'nın yerine kullanılabileceğini göstermiştir.

ACKNOWLEDGEMENTS

I gratefully thank to Prof. Dr. Alper YILMAZ for his supervision throughout my studies. It was an incredible experience to have him as my supervisor. He has been very important for my scientific and personal development during my M.Sc. studies. He gave me the necessary opportunity and responsibility, support and thrust which were very crucial for my studies.

I sincerely thank to Prof. Dr. Kadir AYDIN for sharing his knowledge and valuable time for this work.

I would like to thank to all Automotive Engineering Department academic personals Prof. Dr. Ali KESKİN, Assoc. Prof. Dr. Abdülkadir YAŞAR, Assoc. Prof. Dr. Mustafa ÖZCANLI, Assoc. Prof. Dr. Mehmet BİLGİLİ, Assoc. Prof. Dr. Hasan SERİN, Asst. Prof. Dr. M. Atakan AKAR, Asst. Prof. Dr. Tayfun ÖZGÜR and Specialist Dr. Ceyla ÖZGÜR.

I would like to thank my friends Ress. Asst. Oğuz BAŞ, Ress. Asst. Şafak YILDIZHAN, Nursima BÜYÜK, Mehmet Can Pektaş and all staff of Automotive Engineering Department at Çukurova University for their continuous support and motivation.

Finally, I would like to thank to my most valuable possession; parents and sister. They encouraged me, worried about me, gave me the necessary support throughout my life. I certainly would not have succeeded to finish my thesis without their support.

CONTENTS **PAGE**

LIST OF TABLES **PAGE**

LIST OF FIGURES **PAGE**

LIST OF ABBREVIATIONS AND NOMENCLATURE

ALT	Atmospheric Life Time
CFC	Chlorofluorocarbons
CI	Compression Ignition
CO_2	Carbon dioxide
COP	Coefficient of Performance
EES	Engineering Equation Solver
EPA	Environmental Protection Agency
GWP	Global Warming Potential
h	enthalpy
HCFC	Hydrochlorofluorocarbon
HFC	Hydrofluorocarbons
HFO	Hydrofluoroolefin
HV	High Value
IHE	Internal Heat Exchanger
LV	Low Value
$\dot{M}$	mass flow rate
MV	Medium Value
ODP	Ozone Depletion Potential
ORC	Organic Rankine Cycle
ORVC	Organic Rankine vapor compression cycle
P	pressure
s	entropy
SI	Spark Ignition
T	temperature
T-ORC	Transcritical ORC
T-ORVC	Transcritical ORVC

UV	Ultraviolet
VCC	Vapor Compression Cycle
w	work
η	efficiency

Superscripts and Subscripts

boil	boiler
con	condenser
eva	evaporator
H	high
L	low
ref	refrigerant
sub	subcooling
sup	superheating
t	turbine
th	thermal

1. INTRODUCTION

Recently, waste heat utilization has attracted much more interest due to the limited amount of fossil fuels and environmental damages as a result of their usage. Researchers have studied on several cycles such as, thermoelectric, sorption (absorption and adsorption), triangle, desiccant Kalina and organic Rankine cycle (ORC). ORC has the flexibility w to delivered mechanical power by the expander/turbine, which can utilize thermal energy without interruption all year round (Li et al., 2013). ORC is also a widely used technology. It can be used in local and small-scale applications unlike traditional Rankine cycles. It has the benefit of utilizing large range of temperature heat sources for example from 75 to 525 ºC (Wang et al., 2011; Capata and Toro, 2014). High amount of waste heat energy is recovered by ORC when compared to other cycles (Li, 2016).

For Rankine cycle, working fluids can be CO_2, ammonia, water or organic substances. Among them, organic fluids are desirable for low grade thermal energy utilization (Li et al., 2013). Besides, organic working fluids have lower boiling point, higher molecular mass and higher mass flow when compared to water. These given properties makes turbine efficiency of ORC higher than that of steam Rankine cycle (Eyidogan et al., 2016).

In the mobile air conditioning industry, R12 was replaced with R134a to avoid further destruction of ozone layer in 1990s after the Montreal protocol. Although, R134a has zero ozone depleting potential (ODP), it is a greenhouse gas due to having high glabal warming potential (GWP). It is also stated that, R134a may be decomposed by sunlight in the troposphere and cause acidic and poisonous substances. This may cause more serious disaster than CFC made. Use of R134a is restricted after Kyoto protocol came into force (Bolaji and Huan, 2013; Zhao et al., 2012). Thus, a replacement of R134a is required with more environmental friendly refrigerants.

The refrigerant that replaces R134a must primarily fulfill the following requirements:

- It must have a GWP lower than 150 to comply with the EPA standarts.
- Pressure-Temperature diagram should correspond to the P-T diagram of R134a
- It should not be flammable and have low toxicity level.
- It must have low atmospheric life. It is known that atmospheric life of R134a is more than ten years.

Studies are showed that best satisfactory alternatives of R134a are R1234yf and R1234ze(E) (Yataganbaba et al., 2015). Both refrigerants have zero ODP, very low GWP, low toxicity and mild flammability level (Molés et al., 2015a). Additionally, they can operate at similar conditions (Mota-Babiloni et al., 2014).

Table 1.1. Various engine types and their power output (Jadhao and Thombare, 2013)

Engine type	Power Output (kW)
Small air cooled diesel engine	35
Small agriculture tractors and construction machines	150
Water air cooled engine	35-150
Earth moving machines	520-720
Marine applications	150-220
Trucks and road engines	220

Internal combustion engines utilize rougly one third of the fuel energy. It means that rest 60-70 % of the enegy is released to the atmosphere as a waste heat (Zhao et al., 2014). Average temperature range of exhaust gas changes between 500-600 °C with a maximum value of 1000 °C depending on engine type,

operation conditions and location of the temperature-measuring device (Armstead & Miers 2010). It can be inferred from table 1.1. that, there is a great amount of wasted power potential to be recovered.

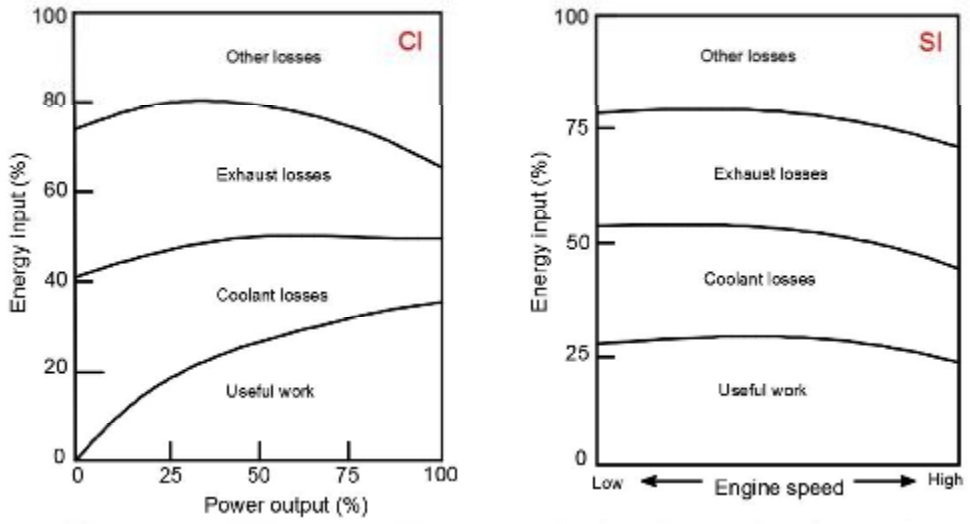

Figure 1.1. Heat balance diagram for a typical CI and SI engine (Ganesan, 2012)

There are several benefits of waste heat recovery (Jadhao and Thombare, 2013):

- Reduction in fuel consumption: Waste heat recovery enhance the efficiency of combustion process.
- Reduction in air pollution: Exhaust gases such as carbon monoxide, nitrogen oxides, hydrocarbons, and particulate matter are reduced through retrieval of heat.
- Reduction in equipment size: As a result of lower fuel consumption, size of flue gas treatment system is reduced.

In this thesis, low grade exhaust waste heat utilization of internal combustion engines via T-ORVC system using low GWP refrigerants is investigated in order to obtain cooling. In ORC side, there is a waste heat-refrigerant heat exchanger. Turbine of ORC and compressor of vapor compression cycle (VCC) is coupled with a shaft. Both cycle use a common condenser and same working fluid. Only waste heat of exhaust gas is regarded as heat source. These modifications simplified the cycle construction giving higher reliability and low maintenance. Low GWP refrigerants R1234yf and R1234ze(E) are considered as alternatives for high GWP refrigerant R134a. Coefficient of performances of these refrigerants are compared over wide range of operation conditions.

2. PRELIMINARY WORK

Investigation on Rankine cycles for engine waste heat recovery dates back to 1970, era of the first energy crisis erupted (Zhu et al., 2013). Fazeli et al. (2011) theoretically presented the combination of Rankine and absorption refrigeration cycle using artificial neural network to simulate thermodynamic properties. In order to obtain both cooling and power, one cooling heat exchanger and two individual turbines were applied to the system (Fazeli et al., 2011). Demirkaya et al. (2011) investigated the Goswami Cycle, which is the combination of Rankine and absorption refrigeration cycles using Chemcad simulation software. Optimum conditions for various ammonia concentrations, boiler pressure and isentropic turbine efficiency were obtained (Demirkaya et al., 2011). Rashidi et al. (2011) developed a study on transcritical power cycle using different types of working fluids. They used artificial neural networks and genetic algorithms to make optimization for first law, exergy efficiency and net work output value. It was seen that these values reached maximum point subsequently, and they decreased with the increase in turbine inlet pressure (Rashidi et al., 2011). Popli et al. (2012) presented feasibility of a Combined Cooling, Heating and Power (CCHP) generation system in a technical and economical manner. Thermodynamic analysis was performed using engineering equation solver (EES). Theoretical study showed that 79.7 MW of waste heat could be recovered providing 45 MW of cooling (Popli et al., 2012).

ORC, having the same components as Rankine cycle, utilizes organic fluids instead of water. In ORC systems, turbines are less complicated due to the lower enthalpy loss. Higher efficiencies are acquired at part loads (Shu et al., 2014). Roy et al. (2010) performed a parametric study of ORC at superheated and constant pressure of 25 bar using engineering software MATLAB. Refrigerants R123, R134a, R12 and R717 were examined as working mediums. Among these refrigerants, R123 yielded highest turbine work, availability, first and second law

efficiencies with lowest irreversibility. Results also revealed that total irreversibility of the system is increased with increasing turbine inlet temperature (Roy et al., 2010). Capata et al. (2014) made a preliminary feasibility analysis for automotive application of ORC recovery system. CAMEL-Pro software was applied for simulation of the proposed system. For a sport sedan car with engine compartment dimensions of 1.10 x 1.20 x 0.80 m^3 (1056 dm^3), proposed ORC system dimensions were determined as 1.03 x 0.83 x 0.40 m^3 (341 dm^3) (Capata and Toro, 2014). Yang and Yeh (2014) investigated the ORC system to retrieve waste heat from cylinder jacket water of large marine diesel engines using low GWP refrigerants. System was operated at the temperature ranges of 58-68 °C and 35-45 °C for boiler and condenser, respectively. Refrigerants which show performance from best to worst are R600a, R1234ze, R1234yf, R245fa, R245ca, and R1233zd (Yang and Yeh, 2014). Zhang et al. (2015) presented a theoretical comparison of three cycle configurations considering ORC as a bottoming cycle, using high temperature waste heat. These cycles were dual-loop ORC, Brayton-ORC and thermoelectric generator-ORC. Among these cycles, dual loop ORC had the highest energy utilization capacity (Zhang et al., 2015). Macián et al. (2013) proposed a design methodology for waste heat recovery optimization of heavy-duty diesel engine. Waste heat sources, exhaust gases, EGR, aftercooler, intercooler and cooling water were compared in terms of total power and exergy performance. After the optimization, approximately 5% maximum improvement in bsfc was obtained (Macián et al., 2013). Shu et al. (2014a) conducted a theoretical study on diesel engine waste heat with bottoming ORC for alkane based working fluids at different boiler temperature under different pressures. REFPROP software was used for calculations. It was concluded that fluids which contained higher number of carbon atoms in their chain, had better power output, thermal efficiency and lower exergy destruction rate (Shu et al., 2014a). Shu et al. (2014b) developed a multi-approach evaluation system exploiting both jacket water and exhaust gas waste heat. It was stated that transcritical ORC system was much better than

subcritical ORC. It was also pointed out that dual loop ORC system was relatively convenient for waste heat recuperation (Shu et al., 2014b). Yu et al. (2013) conducted a simulation model of ORC. In that study recovered waste heat from exhaust and jacket water were 75% and 9.5%, respectively. Simulation results showed that, engine thermal efficiency can be as high as 6.1% using proposed ORC system (Yu et al., 2013). Zhu et al. (2013) presented a thermodynamic model of ORC in Matlab software using five different working fluids. The result showed that the internal exergy destruction of the boiler decreased as the boiler pressure increased (Zhu et al., 2013). Zhang et al. (2011) performed experiment on ORC system assembled on Toyota 8A-FE gasoline engine using R113 as working fluid. The outcomes indicated that exergy range was 45-70% while the thermal efficiency value gain was 14.44% (Zhang et al., 2011). Wang et al. (2012) made a comperative study of different waste heat recovery system configurations named as simple ORC, ORC with IHE, ORC with open and closed feed organic fluid heater and ORC with a reheater. After feasible working region was determined, thermal efficiency of each configuration was maximized using genetic algorithm. Among the evaluated configurations, ORC with IHE showed the best overall performance (Wang et al., 2012). Katsanos et al. (2012) developed a theoretical model of ORC regaining heavy-duty truck diesel engine waste heat. R245ca and water were regarded as working mediums. Study stated that obtained bsfc range was from 10.2% to 8.5% for R245ca and from 6.1% to 7.5% for water as working fluid with increasing engine load from 25% to 100% (Katsanos et al., 2012). Campana et al. (2013) made an estimation study of ORC application in cement, glass, steel and oil/gas industries from 27 countries of the EU. Results highlighted that, recovered thermal energy per year was 20000 GWh and prevented CO_2 emission amount was 7.6 M tons (Campana et al., 2013). Yang (2016) carried out an optimization study of transcritical ORC utilizing large marine diesel engine waste heat. R134a, R1234yf, R1234ze, R152a, R152a, R236fa and R290 are considered as working fluids. Results showed that R152 has the highest thermal efficiency and net power

output while R1234yf with the lowest critical temperature has the highest available efficiency among the studied working fluids (Yang, 2016).

Several studies have been implementing related to combined refrigeration and ORC. Wang et al. (2011) proposed a concept of low grade waste heat activated combined ORC and VCC. Refrigerant R245fa and R134a were selected in power cycle and cooling cycle, respectively. Selecting dual fluid system has two main advantages which led to smaller and portable overall system design. Developed system had 4.4 kW cooling with a value of 0.48 COP (Wang et al., 2011). Aphornratana and Sriveerakul (2010) performed a theoretical analysis of ORC and VCC combined with expander-compressor unit consist of two free piston devices. Boiler temperature range and condenser temperature range were 60-90 °C and 30-50 °C, respectively. Calculated COP value was varied between 0.1 and 0.6 (Aphornratana and Sriveerakul, 2010). Wang et al. (2011) presented different cycle configurations of ORC-VCC. Firstly, a subcooler was added between condenser and expansion valve. Secondly, a cooling recuperator was added after subcooler in order to get more subcooled fluid and thereby to obtain an advanced cycle. Compared to basic cycle, advanced cycle had a subcooler and a cooling recuperator. With these modifications, 22% of improvement on gross COP was obtained by advanced cycle compared to basic cycle (Wang et al., 2011). Aneke et al. (2012) made theoretical comparison of ORC driven VCR and Absorption Refrigeration (AR) system. IPSEpro software was used for modelling and simulation of the cycles. NH_3-H_2O was selected as working medium. Obtained COP values of ORC driven VCR and AR system were 0.57 and 0.55, respectively. In addition, ORC driven VCR system showed better second law performance with 0.727 kW/K energy dissipation than AR system with 1.112 kW/K. The result of the analyses proved that ORC driven VCR system had better thermodynamic performance than AR system (Aneke et al., 2012). Karellas and Braimakis (2016) stated a thermodynamic model of cogeneration and trigeneration ORC-VCC hybrid system utilizing biomass and solar energy using R245fa as working medium.

Calculations were made for subcritical operation pressures. For a typical apartment block, 12% of fuel and electricity consumption save was obtained with a payback period of 7 years. Maximum thermal efficiency of 5.5% was assesed at 90 °C boiler temperature (Karellas and Braimakis, 2016). Li et al. (2013) presented a mathematical model of ORC powered VCR system using R290, R600, R600a and R1270 as working fluids and calculated the performance of each fluid under different conditions. Results indicated that, overall COP is increased with decreasing working fluid mass flow rate per kW cooling capacity. In addition, R600 showed the best performance among the studied working fluids (Li et al., 2013). Abed et al. (2013) performed the parametric analsis of combined Rankine and absorption refrigeration cycle using propane-decane mixture as an organic working fluid. Presumed turbine inlet pressure, superheated temperature and condenser temperature were 29.5 bar 136.8 °C and 113.4 °C, respectively. Results showed that thermal efficiency was increased with cooling capacity (Abed et al., 2013). Kim et al. (2015) presented thermodynamic performance simulation of ORC-VCC using eight different working fluids. Turbine inlet pressue, turbine inlet temperature and flow division ratio were used as parameters. Result showed that working fluids which have higher critical temperatures exhibits higher thermal efficiency except one working fluid (Kim and Perez-Blanco, 2015). Bu et al. (2013) carried out thermodynamic model of combined ORC-VCC ice maker powered by solar energy using R123, R245fa, R600a and R600 as working fluids. Among these working fluids, R600 and R600a had higher efficiencies for ORC side and has higher COP values for VCC side. Results showed that R124 has the highest COP value as well as overall efficiency (Bu et al., 2013). Moles et al. (2015a) examined the computational analysis of ORC-VCC using low GWP refrigerants. It was determined that COP value, which was in between 0.30 and 1.10, increased with recuperator effectiveness and boiler temperature and decreased with condenser temperature (Molés et al., 2015a). Yue et al. (2016) performed thermal and economic analysis of ORC coupled vapor compression

refrigeration system for vehicular application employing R134a, R245fa and cyclopentane. Provided thermal efficiency of the system was ranged from 9.2 to 9.8% and a corresponding diesel fuel saving per hour was ranged from 1.1 to 1.3 L. Study also emphasized that R134a gave the best thermal and economical results (Yue et al., 2016). Sarr and Mathieu-Potvin (2016) studied on different ORC-Refrigeration cycle combinations to increase the efficiency of power systems, which relied on Rankine cycles. Unlike conventional Rankine-Refrigeration combinations, the objective of the study was rejecting heat from Rankine cycle to refrigeration cycle instead of releasing heat directly to environment in order to create low temperature heat sink (i.e. lowering condenser temperature) for Rankine cycle before the pumping step. Rankine and refrigeration cycles with 84x84 fluid combinations were studied. Among these 7056 possible combinations, 2878 were applicable for new concept, which provided improvement in the efficiency up to 2.2% (Sarr and Mathieu-Potvin, 2016). Nasir and Kim (2016) made a theoretical study on thermal performance of ORC powered VCC for domestic usage. Combinations of working fluids of R134a, R245fa, R123, R1234yf, R1234ze(E), Butane and Isobutane were analysed for power and refrigeration sides. Combinations of R134a and Isobutane for ORC and VCC, gave the best performance, which had total COP values between 0.172 and 0.217, respectively. Furthermore, R134a and its possible substitutes R1234yf and R1234ze gave the best results for ORC side (Nasir and Kim, 2016). Saleh (2016) presented a parametric study of a combined ORC-VCR activated by low-grade heat. Proposed refrigerants of this study were R1270, R290, RC318, R236fa, R600, R236ea, R600a, R245fa, R1234ze(E), and R1234yf. In addition to expander and compressor efficiencies, condenser, evaporator and boiler temperatures were used as parameters. Result of the study pointed out that R600 and R245fa show the highest COP values (Saleh, 2016). Yue et al. (2015) made performance comparison of two cycle Kalina and Transcritical ORC for engine exhaust waste heat recovery. Alkane based working fluids pentane, hexane, heptane, octane, nonane and decane

selected for Transcritical ORC, zeotropic ammonia-water mixture was used for Kalina cycle. Compared to Kalina cycle, T-ORC showed substantially better overall waste heat recovery efficiency. For T-ORC, obtained optimum exhaust temperature range was 296-345 °C at 40-60% ICE load (Yue et al., 2015). Zhao et al. (2012) presented an experimental analysis of a mobile air conditioning system using R1234yf and R134a as working media under different heat and load conditions. The study highlighted that, COP of R1234yf is only 9% lower than that of R134a (Zhao et al., 2012). Zilio et al. (2011) conducted numerical simulations using R1234 for European automotive air conditioning system. Results revealed that COP values of R1234yf can be larger than that of R134a increasing the surface area of the condenser by 20%, and one of the evaporator by 10% and utilizing overridden compressor (Zilio et al., 2011).

3. MATERIAL AND METHOD

3.1. Refrigerant Selection

3.1.1. Progress of Refrigerants

Since the industrial revolution, there are four generations of refrigerants (Calm, 2008).

1) First Generation - Whatever worked (1830-1930): During this time period, refrigerants include familiar solvents and other volatile fluids. Almost all those refrigerants were toxic, flammable and some of them highly reactive causing accidents frequently. (i.e. NH_3, CO_2, SO_3, $HCOOCH_3$, H_2O, CCl_4 and CHCS)
2) Second Generation - Safety and durability (1931-1990): This time period, refrigerants were comprised of chlorofluorocarbons, ammonia, hydrochlorofluorocarbon and water. Ammonia was the most popular refrigerant of this generation.
3) Third Generation - Ozone protection (1990-2010s): Montreal protocol was signed due to destruction of ozone layer. Thus, transition to ozone friendly refrigerants were took place. This time period, refrigerants are comprised of hydrofluorocarbons, CO_2, water and hydrocarbons.
4) Fourth Generation - Global Warming (2010-?): Due to global warming, F-gas regulation is adopted. Refrigerants of the fourth generation should have zero or very low ODP, low GWP and high efficiency. Potential refrigerant candidates of this generation are low GWP hydrofluorocarbons, natural refrigerants such as ammonia, CO_2, water and unsaturated hydrofluorochemicals (Calm, 2008).

3.1.2. Chemical Classification of Refrigerants

In the following section, refrigerants are classified according to their chemical composition.

3.1.2.1. Chlorofluorocarbons

A chlorofluorocarbon (CFC) is an organic compound which comprises volatile derivatives of methane and ethane in combination with halogenated elements like fluorine and chlorine. CFCs are artificially manufactured compounds. Thus, the common formula of CFCs can be indicated as CCl_nF_{4-n} and $C_2Cl_nF_{6-n}$ with non-zero value of "n" (Kim et al., 2011). CFCs are also named as Freon^{TM} by the The Dupont company (Ahrens, 2003). They are nonflammable, nonexplosive, noncorrosive, odorless, nonirritating, non-poisonous and inert at ordinary temperatures (Maunder et al., 1992; Schnubel, 2009).

There are mainly two types of CFCs; fully halogenated and partially halogenated. Expecially fully halogenated types of CFCs are comprise solely of carbon and halogens; therefore, have high ODP (Maunder et al., 1992). Chlorine content of CFCs is primarily responsible for ozone depletion. As CFCs are released into atmosphere, dissociation occurs by the UV light to release free chlorine. Free chlorine atom decomposes ozone molecule giving oxygen gas and then regenerates itself as follows (Hardcover, 2011):

$$CF_2Cl_2 \rightarrow CF_2Cl + Cl$$
$$Cl + O_3 \rightarrow ClO + O_2$$
$$ClO + O \rightarrow Cl + O_2$$

As a consequence, Montreal protocol was signed in 1987 to regulate the manufacturing and distribution of CFC's (McConnell and Abel, 2015).

3.1.2.2. Hydrochlorofluorocarbons

Hydrochlorofluorocarbons (HCFCs) are the subclass of CFCs in which at least one of chlorine or fluorine atom is substituted by hydrogen atom (Akimoto, 2016). Hydrochlorofluorocarbons (expecially HCFC-124) are used as a substitude for CFCs as a result of Montreal protocol implementation (Kaplowitz, 2013). HFCSs are also less toxic than CFCs in addition to being more ozone friendly. Neverthless, HCFCs are still regarded as greenhouse gas and they are planned to be phased out by the year 2020. Today, Refrigeration system of trucks and reefers utilizes HCFCs (Bennett, 2015).

3.1.2.3. Hydrofluorocarbons

Hydrofluorocarbons (HFCs) are fundamentally developed as a replacement of CFCs. HFCs don't contain chlorine; hence, have no damage to stratospheric ozone layer. In addition, they have shorter atmospheric life due to the presence of hydrogen atom(s). Thus, they have lower GWP value than CFC compounds. After the phase out of CFCs by Montreal protocol, production rate of HFCs has been rising. Large number of fluorine atoms makes HFCs nonflammable, less toxic, stable to heat energy and less reactive (Voogt, 2012; Anonymus, 2011).

In mobile air-conditioning, automobile industry turned to HFCs, mainly to HFC-134a (R134a) in the mid 1990s in order to replace the ozone destroyer CFC-12. Even though R134a doesn't deplete ozone layer, each unit mass of the compound has the global warming potential (GWP) of 1430. As a consequence, annually refrigerant leakage originated from vehicle air conditioners releases 53 tons of CO_2 to the environment (Cox, 2012). In 1997, Kyoto protocol was signed to reduce the six specified types of gases which are known as CO_2, methane, HFCs, nitrous oxide, perfluorocarbons, and sulfur hexafluoride (Smith, 2006).

3.1.2.4. Hydrofluoroolefins

Fourth generation refrigerant Hydrofluoroolefins (HFOs) with zero ODP and low GWP are composed of hydrogen, fluorine and carbon atoms. The first HFO developed by Honeywell and Dupont, is R1234yf that have the brandnames SOLSTICE yf and Opteon YF. This low GWP refrigerant is introduced to automotive industry as a replacement for R134a (Anonymous, 2016).

3.1.3. Toxicity and Flammability of Refrigerants

ASHRAE standart 34, categorises frequently used refrigerants depending on their toxicity and flammability. There are mainly six safety groups, A1, A2, A3, B1, B2 and B3, which describe the level of flammability and toxicity. The "A" denotes where toxicity levels haven't been identified at concentrations less than or equal to 400 ppm (parts per million) and "B" where evidence of toxicity level is less than 400 ppm. "1" denotes no flame propogation when tested in 18.3 ºC air at 1.01 bar, "2" lower flammability limit of higher than 100.115 g/m^3 when tested at 21.1 ºC, 1.01 bar and "3" defines higher flammability where flammability limit is lower than or equal to 52.22019 g/m^3 at 21.1 ºC, 1.01 bar and "L" letter of the two subclass (A2L and B2L) refer to lower flammability (Anon, 2008; Johnson, 2016). Table 3.1. summarizes the refrigerant safety classifications according to American Society of Heating, Refrigerating and Air-Conditioning Engineers (ASHRAE) Standard 34.

Table 3.1. Refrigerant Safety classification (Sarbu, 2014)

	Lower toxicity	Higher Toxicity
Higher Flammability	A3	B3
Lower Flammability	A2	B2
	A2L	B2L
No Flame Propogation	A1	B1

3.1.4. Saturation Vapor Curve of Refrigerant T-s Diagrams

Refrigerants can be categorised as a dry, isentropic or wet fluid according to slope (dT/ds) of the temperature-entropy (T-s) diagram. Seeing that, the dT/ds value reaches infinity for isentropic fluids, the inverse of the slope (ds/dT) is desired to indicate how dry or wet the fluid is. The value of ξ=ds/dT classifies the fluids as follows (Chen et al., 2010):

$\xi > 0$: dry fluid
$\xi < 0$: wet fluid
$\xi \approx 0$: isentropic fluid

The saturation curve is an important criteria for selection of working fluids. In general, dry and isentropic working fluids show better thermal performance. Because at the end of the expansion process, wet fluid condenses; thus, formation of droplets occur. On the other hand, dry and isentropic fluids don't condense (Li, 2016; Quoilin et al., 2012). Neverthless, if the working fluid is too dry, vapor will be highly superheated and cause an extra cooling load for condenser. which is a waste after the expansion through the turbine (Chen et al., 2010). Figure 3.1. shows the typical T-s diagrams of wet, dry and isentropic working fluids.

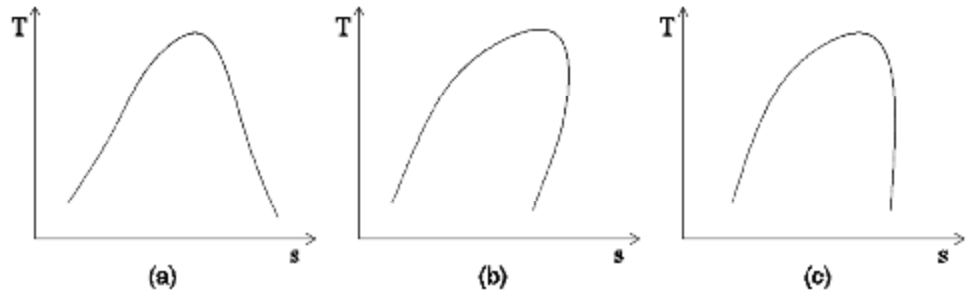

Figure 3.1. T-s diagrams of (a) wet, (b) dry and (c) isentropic refrigerants

3.1.5. Selected Working fluids

Selecting of working fluid is crucial for the system to achieve high thermal performance utilizing convenient heat source efficiently (Li, 2016). There is a wide range of working fluids. Selected working fluid should have the following characteristics in addition to having low ODP and GWP (Quoilin et al., 2012):

- Positive or isentropic saturation vapor curve: Working fluid should be superheated after expansion in the turbine to avoid the turbine damages.
- High vapor density: This is an important parameter particularly for fluids which have low condensing pressure. Lower density cause higher flow rate thus, increased pressure drop in the heat exchangers. Because of this, larger expander should be selected.
- Low viscosity: In order to compensate for low viscosity, high heat transfer coefficients and low friction losses are required in the heat exchangers.
- High stability temperature: High temperature causes decomposition and chemical deteriorations. Therefore, working fluid should have high decomposition temperature.
- High safety level: As stated in previous section, working fluid should have low flammability and low toxicity.
- Easy availability and low cost.

Table 3.2. Environmental properties of some common refrigerants (Bolaji and Huan, 2013)

Compositional Group	Refrigerant	ODP	GWP	Safety Group
CFCs	R11	1	3800	A1
	R12	1	8100	A1
	R113	0.8	4800	A1
	R114	1	9000	A1
	R115	0.6	9000	A1
HCFCs	R22	0.055	1500	A1
	R123	0.02	90	B1
	R124	0.022	470	A1
	R141b	0.11	630	A2
	R142b	0.065	2000	A2
HFCs	R23	0	11700	A1
	R134a	0	1430	A1
	R125	0	2800	A1
	R143a	0	3800	A2
	R152a	0	140	A2
Natural Refrigerants	R290	0	3	A3
	R600a	0	3	A3
	R717	0	0	B2
	R718	0	0	A1
	R744	0	0	A1
HFOs	R1234yf	0	<1	A2L
	R1234ze(E)	0	<1	A2L

Although, there is no refrigerant that satisfies all the criteria, R1234yf and R1234ze(E) are the best candidates as an alternative to R134a.

Table 3.3. Thermophysical properties of studied refrigerants (Molés et al., 2015b)

Properties	R134a	R1234yf	R1234ze(E)
Chemical Formula	$C_2H_2F_4$	$CF_3CF=CH_2$	$CHF=CHCF_3$
Critical temperature (ºC)	101.06	94.7	109.37
Critical pressure (MPa)	4.06	3.38	3.64
Molecular Weight	102	114	114
Slope	Isentropic	Isentropic	Isentropic
ALT (year)	13.4	0.0287	0.0274
Normal Boiling point (ºC)	-26.36	-29.78	-19.25

3.2. Heat Recovery Cycles for low to high grade heat sources

3.2.1. Goswami cycle

Goswami cycle is a thermodynamic cycle, which is the combination of a Rankine cycle and absorption cooling cycle. It produces both power and refrigeration simultaneously. The cycle was proposed by Yogi Goswami et al. in late 1990s. Studies have been undergoing since that time (Demirkaya et al., 2011).

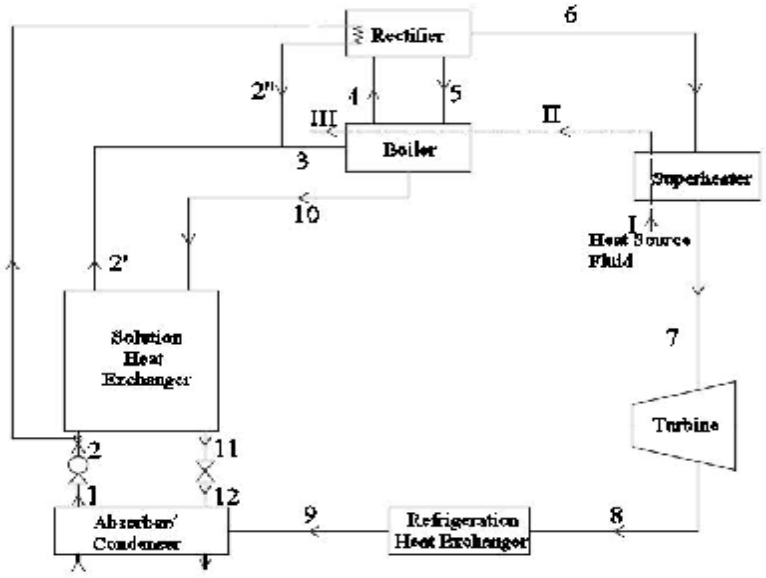

Figure 3.2. Schematic view of ammonia-based Goswami cycle

At first, the cycle is proposed to utilize the mixture of ammonia and water while its primary objective is to produce power. This cycle can be used to recover low-grade heat sources such as solar and geothermal energy. System requires the following equipments: absorber, heat recovery, turbine, heat exchangers and boiler (Demirkaya and Goswami, 2011). Schematic description of Goswami cycle is illustrated in Figure 3.2.

Process of the ammonia-based Goswami cycle is follows: Ammonia-water mixture as a relatively strong solution leaves the absorber as a saturated liquid at relatively low pressure. After pumped to a high-pressure mixture is preheated before entering the boiler. While the boiler operates between the bubble and dew point temperatures of the mixture at high pressure, partial boiling produces a high concentration saturated vapour and comparatively low concentration saturated liquid. The weak liquid solution releases heat in the recovery unit then is throttled in the direction of absorber. In order to purify further, the rectifier condenses water while rejecting heat to secondary strong solution stream. In order to produce work, the vapour is superheated and expanded through the turbine. Because of the low boiling point of the ammonia, the vapour expands to low temperatures providing refrigeration potential. Finally, the vapour is absorbed back towards the liquid while releasing heat (Patel, 2013).

3.2.2. Kalina Cycle

Kalina cycle is developed in the late 1980’s by Alexander Kalina in order to convert heat energy into mechanical energy. It utilizes ammonia-water mixture. The ammonia-water mixture has the advantage of varying condensing and evaporating temperature at supercritical pressures unlike pure fluid, which evaporates and condenses at constant temperature. Kalina cycle uses distinct Distiller Condenser Sub-System (DCSS) to carry out condensation process of the mixture at low pressure by altering ammonia-water mass fraction (Wang et al., 2013).

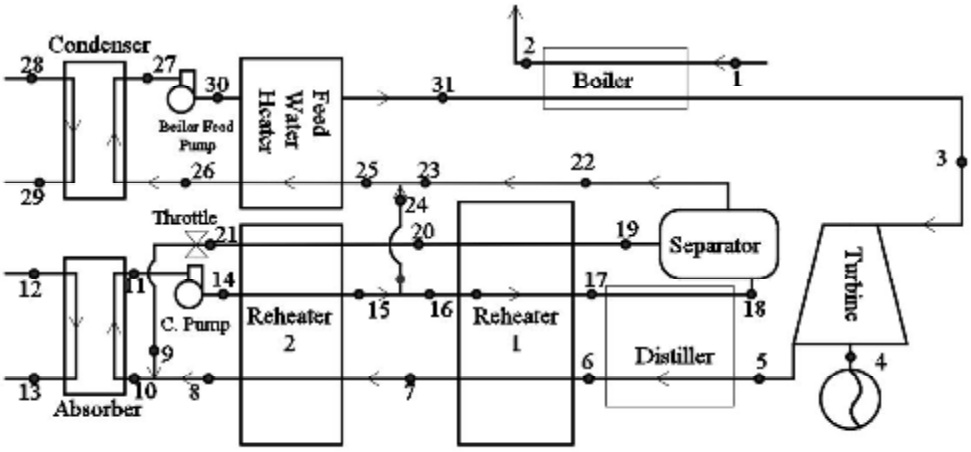

Figure 3.3. Schematic view of simplified Kalina cycle

A basic Kalina cycle process is showed in figure 3.3. The cycle consists of boiler, turbine, distiller, separator, reheater, absorber, condensate pump, throttling valve, condenser, boiler feed pump and feed water heater. Point 1 to 2 represents exhaust gases flowing through the boiler. Superheated ammonia-water mixture at point 3 is expanded in the turbine generating shaft power at point 4. After the turbine at point 5, mixture is cooled through the points 6, 7, 8 and then, it is diluted by ammonia-poor liquid through the points 9, 10 and condensed in the absorber with the help of cooling water (12, 13). After leaving the absorber, saturated liquid at point 11 is pressurised by the condensate pump to medium pressure and then heated. After the point 18 saturated mixture is separated into ammonia-poor liquid. Liquid is cooled in the reheater 2 then depressurised in the throttling valve and then ammonia-rich vapour is cooled at reheater 1. In order to obtain about 70% ammonia concentration, at point 24, some of the condensate is added to ammonia vapour which is practically poor, then point 25 is obtained. The mixture is cooled in the boiler feed water heater unit and condensed by the cooling water and point 27 is reached. After the condensation, mixture is compressed in the feed pump and

reached the boiler with the aid of feed water heater and point 31 is obtained (Zhang et al., 2012).

3.2.3. Ideal Rankine Cycle

Rankine cycle is a thermodynamic cycle which converts thermal energy into shaft power. It is also called as Clausius Rankine Cycle. The main difference between traditional steam rankine cycle and ORC is the working fluid. Traditional steam rankine cycle uses only water as working fluid. All processes are reversible.

The ideal Rankine cycle comprises the following four process, as shown in figure 3.4.:

Process 1-2: Reversible Isentropic compression in the pump
Process 2-3: Constant pressure heat addition in the boiler
Process 3-4: Reversible Isentropic expansion in the turbine
Process 4-1: Constant pressure heat rejection in the condenser

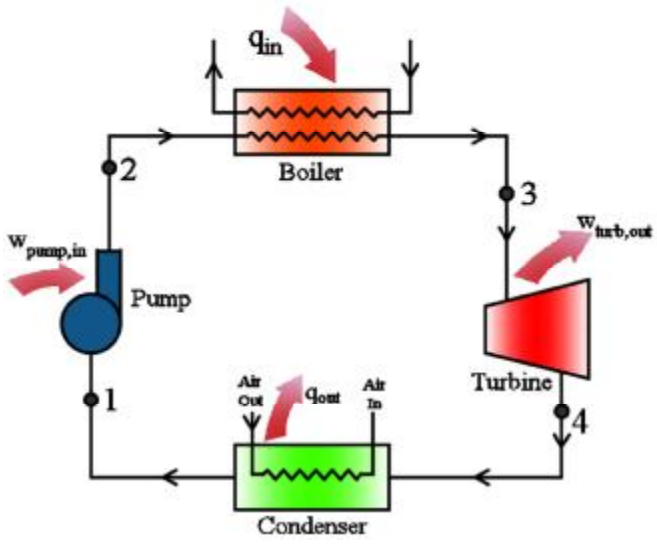

Figure 3.4. Schematic view of ideal Rankine cycle

For an ideal Rankine Cycle, working fluid enters the pump as saturated liquid at point 1. Pump compresses the working fluid isentropically to point 2. During the compression process, water temperature increases slightly due to the decrease in specific volume.

High-pressure working fluid enters the boiler at point 2. Boiler superheats the working fluid at constant pressure. Afterwards, working fluid reaches point 3. Superheated working fluid enters the turbine at point 3. Turbine expands the working fluid providing shaft power. After isentropic expansion point 4 reached which is the entrance of condenser. Fluid losses heat during the expansion. Working fluid enters the condenser at point 4. At this point, working fluid is at the saturated mixture region with a high quality. After the condensation at constant pressure point 1 is reached which is on the saturated liquid line. Thus, the cycle is completed.

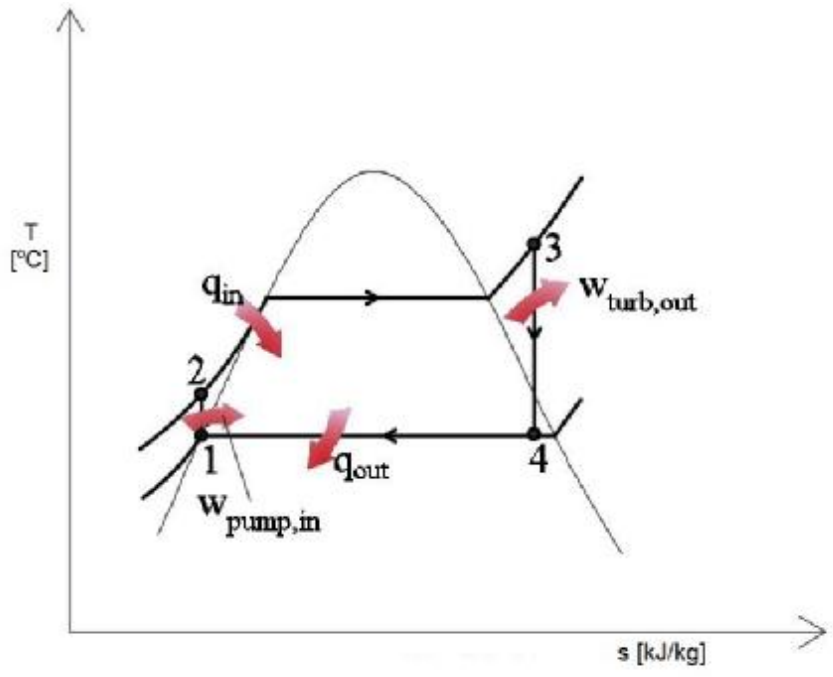

Figure 3.5. Temperature-entropy diagram of Rankine cycle

Figure 3.5. shows the temperature-entropy diagram of a typical Rankine cycle. Enclosed area that is confined to points 1-2-3-4-1 defines the net work done by the cycle.

Energy equation of Rankine cycle for unit mass is given as follows:

$$h_e - h_i = (q_{in} - q_{out}) + (w_{in} - w_{out})$$

While the net work done by the pump is:

$$w_{in(pump)} = h_2 - h_1$$

Net heat addition in the boiler can be calculated by the following equation:

$$q_{in(boiler)} = h_3 - h_2$$

The net work done by the turbine and the heat released from the condenser are determined by the below equations, respectively:

$$w_{out(turbine)} = h_3 - h_4$$

$$q_{out(condenser)} = h_4 - h_1$$

Thermal efficiency of the Rankine cycle is determined using the following equation:

$$\eta_{th(rankine)} = \frac{w_{net}}{q_{in}} = \frac{w_{out(turbine)} - w_{in(pump)}}{q_{in(boiler)}}$$

3.3. Ideal Vapor Compression Refrigeration Cycle

Although, there is a variety of air conditioning systems used in houses, most systems employ vapor compression cycle (VCC) to obtain desired cooling and dehumidification. VCC is also preffered for vehicle air conditioning. First commercial system was manufactured in 1857 by D. E. Siebe and James Harrison (Kreider, 2000). The term vapor compression indicates the utilization of a mechanical compressor (Chiasson, 2016).

Thermodynamically, there are four ideal reversible processes in an ideal VCC, as illustrated in figure 3.6.:

Process 1-2: Isentropic compression in the compressor
Process 2-3: Heat rejection at constant pressure in the condenser
Process 3-4: Throttling in the expansion device
Process 4-1: Heat absorption at constant pressure in the evaporator

For an ideal VCC, refrigerant enters the compressor at point 1. Refrigerant vapor is compressed isentropically to point 2 by the compressor and temperature of the refrigerant is raised after the compression process. Then, the refrigerant enters the condenser at point 2. Superheated refrigerant undergoes cooling. Outside ambient air is colder than the refrigerant at this point. Thus, heat rejection occurs through the condenser, and then point 3 on the saturated liquid line is reached. After, saturated liquid refrigerant enters the expansion device, refrigerant is throttled through the expansion valve and point 4 is obtained. At this point, temperature of the refrigerant is lower than the refrigerated space. Refrigerant enters the evaporator at point 4, which is in the saturated mixture region. It absorbes heat from the environment through the evaporator, and then point 1 is reached which is on the saturated vapor line. Thus, the VCC is completed.

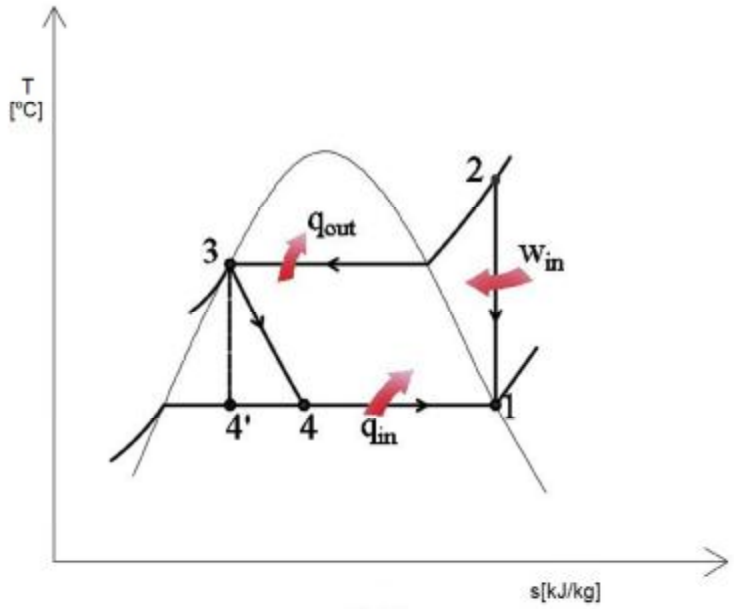

Figure 3.6. Temperature-entropy diagram of Ideal vapor compression cycle

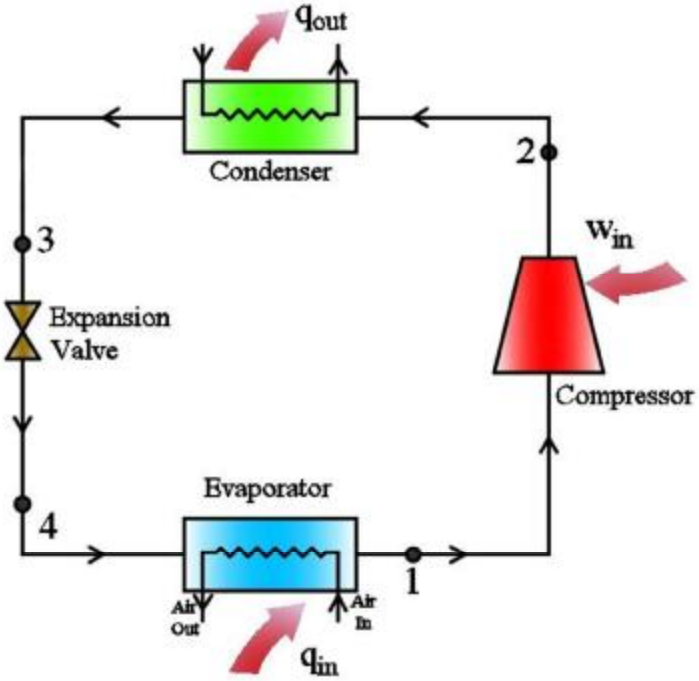

Figure 3.7. Schematic view of ideal vapor compression cycle

All four components of the VCC are steady-flow devices. Thus, steady flow process analyses can be implemented.

The coefficient of performance (COP) can be defined as follows:

$$COP_{ref} = \frac{q_L}{w_{net,in}} = \frac{h_1 - h_4}{h_2 - h_1}$$

3.4. Transcritical Organic Rankine Vapor Compression Refrigeration Cycle

To develop the thermodynamic model, friction and heat losses in T-ORVC refrigeration system are neglected.

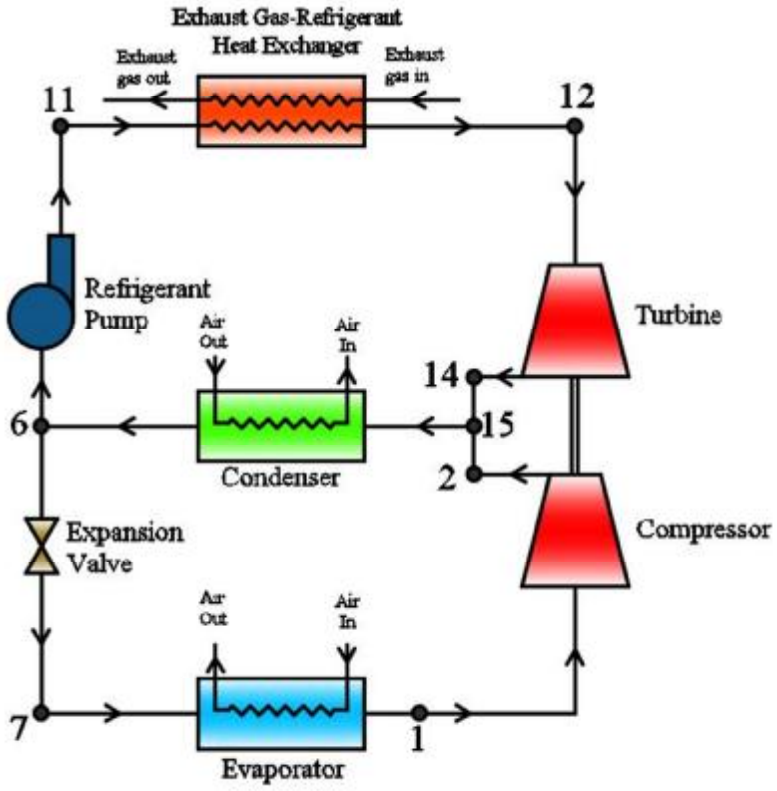

Figure 3.8. Schematic view of T-ORVC refrigeration system

Schematic diagram of the combined T-ORVC refrigeration system is illustrated in Figure 3.8. System process is demonstrated in Figure 3.9. on a pressure-enthalpy diagram. As seen, the system consists of two cycles. ORC cycle labelled as 11-12-14-6-11 and the refrigeration cycle as 6-7-1-2-6. The system basically consists of a refrigerant pump, a pair of heat exchangers, turbine, compressor, evaporator, expansion valve and condenser. Refrigerant at point 6, pumped to a pressure P_{11} which is above the critical pressure P_{cr}. In case of isentropic compression, P_{12} is reached. Afterwards, refrigerant enters the exhaust gas-refrigerant heat exchanger and heated up to temperature T_{12} at constant pressure. The turbine receives the heated high-pressure refrigerant and releases it at condensation pressure P_{14}. In case of isentropic expansion point 13 is reached. Simultaneously, refrigerant coming from evaporation pressure P_1 is compressed to pressure P_2 by the compressor, which is equal to the condenser pressure. In case of isentropic compression, point 3 is reached. Both of the turbine exit and compressor exit fluids combined at point 15 and conveyed through the condenser. Following the condensation at point 5, refrigerant is subcooled to the temperature T_6. Afterwards, liquid line divided into two branches at point 6. First liquid line enters the expansion valve. After the expansion process, point 7 is reached. Following the expansion, refrigerant enters the evaporator. After the evaporation, refrigeration is obtained. Meanwhile, second branch of the fluid from state point 6 enters the refrigerant pump. Therefore, cycle is completed.

Since, the state point at the turbine outlet is very close to saturation curve. recuperator is not required after expansion in the turbine (Schuster et al., 2009).

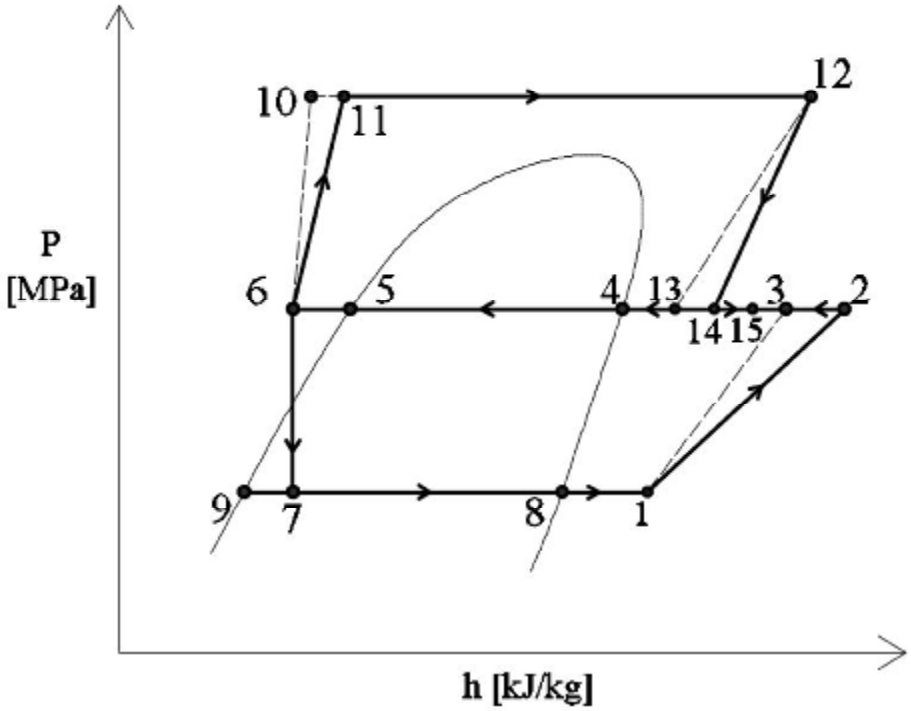

Figure 3.9. Pressure-enthalpy diagram of T-ORVC refrigeration cycle

3.4.1 Thermodynamical Analysis of the System

Temperature of the VCC evaporator is mainly specified by the inlet temperature of the fluid which will be cooled. In order to perform an effective heat transfer, evaporation temperature of the refrigerant T_{eva} is supposed to be 10-15 °C lower than inlet temperature to be cooled.

Likewise, condensation temperature of the refrigerant essentially determined by the cooling fluid. Condensation temperature T_{con} is supposed to be 10-15 °C higher than inlet temperature of the cooling fluid to achieve effective heat transfer.

Corresponding to T_{eva} and T_{con}, subcooling temperature difference ΔT_{sub} between the condenser outlet at point 5 and point 6 and superheating temperature difference ΔT_{sup} between the evaporator outlet at point 8 and point 1 will also be assigned. Additionally, pressure at the outlet of the refrigerant pump and the boiler

temperature at the outlet of the exhaust gas-refrigerant heat exchanger are prescribed, too.

In order to build the analysis, mechanical and isentropic efficiencies of the compressor, turbine and compressor are required. Moreover, pump electromotor efficiency and electricity production efficiency to make comparison between the heat and mechanical work. Yılmaz made a broad literature survey about the cycle component efficiencies stated below. Table 3.4. shows the efficiencies of the compressor, turbine and compressor. Efficiencies are categorised into three groups namely low (LV), medium (MV) and high values (HV).

Table 3.4. High values (HV), medium values (MV) and low values (LV) of system components efficiencies (Yilmaz., 2015).

	η_{ti}	η_{ci}	η_{pi}	η_{tm}	η_{cm}	η_{pm}	η_{pe}	η_{e}
LV	0.70	0.65	0.75	0.95	0.95	0.95	0.90	0.25
MV	0.80	0.75	0.80	0.97	0.97	0.97	0.92	0.30
HV	0.90	0.80	0.90	1.00	1.00	1.00	0.95	0.35

Temperature at the inlet of the compressor T_1 can be determined by the given values T_8 and ΔT_{sup}:

$$T_1 = \Delta T_{sup} + T_8 \tag{3.1.}$$

Similarly, pump inlet temperature, T_6 can be determined by the assigned values T_5 and ΔT_{sub}:

$$T_6 = T_5 - \Delta T_{sub} \tag{3.2.}$$

Using the given values above, h_1, s_1, h_6 and s_6 can easily be calculated. Additionally, compression from point 1 to 3 and 6 to 10 are isentropic at the compressor and at the pump. Thus, following equations can be written as:

$$s_3 = s_1 \tag{3.3.}$$

$$s_{10} = s_6 \tag{3.4.}$$

Since, evaporation pressure P_7 and the pump exit pressure P_{11} are known, enthalpies at point 10 and 3 can be obtained. Therefore, using the following expressions, enthalpies at the compressor and pump outlet can be determined:

$$h_2 = h_1 + \frac{h_3 - h_1}{\eta_{ci}} \tag{3.5.}$$

$$h_{11} = h_6 + \frac{h_{10} - h_6}{\eta_{pi}} \tag{3.6.}$$

After the isentropic expansion through the turbine, enthalpy, h_{13} at the turbine outlet can be calculated using the known values P_{12} and T_{12} at the end of the exhaust gas-refrigerant heat exchanger. Hence, entropy at the turbine outlet can be written as:

$$s_{13} = s_{12} \tag{3.7.}$$

Pressure at point 13 is equal the given value of condensation pressure. Therefore, enthalpy h_{14} at point 14 can be determined using the turbine isentropic efficiency η_{ti}:

$$h_{14} = h_{12} - \eta_{ti}(h_{12} - h_{13}) \tag{3.8.}$$

Expansion in the expansion valve is isenthalpic. Hence:

$$h_7 = h_6 \tag{3.9.}$$

The mechanical efficiencies of the turbine ηt and the compressor ηc are given. Net work generated by the turbine can be calculated by:

$$\dot{W}_t = \dot{M}_t(h_{12} - h_{14})\eta_{tm} \tag{3.10.}$$

Whereas, the work required for the compressor is:

$$\dot{W}_c = \frac{\dot{M}_c(h_2 - h_1)}{\eta_{cm}} \tag{3.11.}$$

Here $\dot{M}_c$ and $\dot{M}_t$ are mass flow rate of the compressor and turbine, respectively. Definition of mass flow rate ratio w is:

$$w = \frac{\dot{M}_c}{\dot{M}_t} \tag{3.12.}$$

Overall efficiency of the compressor and turbine is:

$$\eta_{tc} = \eta_{ti}\eta_{ci}\eta_{tm}\eta_{cm} \tag{3.13.}$$

Using the equations (3.5.), (3.8.) and (3.10.)-(3.13.), following equation for the mass flow rate ratio is determined:

$$w = \eta_{tc}\frac{h_{12} - h_{13}}{h_3 - h_1} \tag{3.14.}$$

Enthalpy of the working fluid at the condenser inlet h_{15} can be obtained as follows:

$$h_{15} = \eta_{tc} \frac{h_{14} + w h_2}{1 + w} \tag{3.15.}$$

The following COP equation only considers obtained heat by the exhaust gas-refrigerant heat exchanger to the working fluid.

$$COPH = \frac{w(h_1 - h_7)}{h_{12} - h_{11}} \tag{3.16.}$$

Next COP equation express the rate of received refrigeration to consumed pump energy;

$$COPW = \frac{w(h_1 - h_7)\eta_{pem}\eta_{pm}}{h_{11} - h_6} \tag{3.17.}$$

where η_{pem} and η_{pm} are electromotor and mechanical efficiency of the pump, respectively. At last, COPT is defined. COPT definition comprises supplied energy of waste heat and supplied heat equivalence energy for the pump:

$$COPT = \frac{w(h_1 - h_7)}{\frac{(h_{11} - h_6)}{\eta_{pem}\eta_{pm}\eta_e} + (h_{12} - h_{11})} \tag{3.18.}$$

Where η_e is electricity production efficiency utilizing heat energy.

EES (Engineering Equation Solver) software is developed to perform the thermodynamic simulation of the introduced T-ORVC refrigeration system with R134a, R1234yf and R1234ze(E) as refrigerants at given parameters. This powerful software includes thermophysical properties of various fluids. It has been widely used to analyse the energy systems, expecially for waste energy recovery (Popli et al., 2012).

4. RESULTS AND DISCUSSION

Simulations are performed within the parameters given in table 4.1. and influence of each one on system coefficient of performance is examined in this section.

Table 4.1. T-ORVC refrigeration system performance parameters.

Parameters	Values
Boiler (exhaust gas - refrigerant heat exchanger) temperature	100-200 °C
Evaporation temperature	0-15 °C
Condensation temperature	45-60 °C
Boiler pressure	30-80 bar
Subcooling/superheating temperature differences	1-5 °C
Component efficiencies	LV, MV, HV

4.1. Validation of Calculations

Although, there is not any research on supercritical system using current working fluids, there is a novel study for subcritical systems given by Saleh (2016). Cycle configuration, which has common condenser for ORC and VCC side, is same as the cycle of this thesis. They used both R1234yf and R1234ze(E) with same COP description as the COPH description of this study. Parameters are set identical as given basic parameters. Though boiler pressure of their study is not given, it is set to 30 bar in order to simulate subcritical condition. According to comparison results given in table 4.1., COP differences given by Saleh and this study for working fluids R1234yf and R1234ze(E) are -6.3 and 0.3, respectively. These results seems satisfactory and it is anticipated that simulations for supercritical region should also give satisfactory results.

Table 4.2. Comparison of the results provided from Saleh, (2016) and this thesis (η_{pi}=0.75, η_{ci}=0.75)

Refrigerant	T_{con} [°C]	T_{eva} [°C]	$\Delta_{sub}/\Delta_{sup}$ [°C]	T_{boil} [°C]	P_{boil}	COP (Saleh, 2016)	COPH of this thesis	Error [%]
R1234yf	40	5	0	80	-	0.317	0.337	-6.3
R1234ze(E)	40	5	0	80	-	0.356	0.355	0.3

4.2. The Effect of Boiler Temperature on total cooling performance (COPT)

In this section, behaviour of COPT curve is inspected as boiler temperature varies. Subcooling/superheating temperature differences are set to 5 °C for all figures.

Next figure shows COPT versus boiler temperature at 15 °C evaporator temperature, 45 °C condenser temperature and 30 bar subcritical pressure using MV efficiencies. It is clear that, increasing boiler temperature has little effect on COPT value. It seen that, R134a yields slightly higher COPT than R1234yf. Besides, R1234ze(E) has the highest COPT value which corresponds to 18% difference to R134a. There is an optimum value for each refrigerant at a certain boiler temperature. R134a and R1234ze(E) gives the top COPT value in the range of 130-135 °C. As for R1234yf, it yields the top COPT value at about 115 °C. Maximum COPT values are 0.478, 0.464 and 0.5674 for R134a, R1234yf and R1234ze(E), respectively.

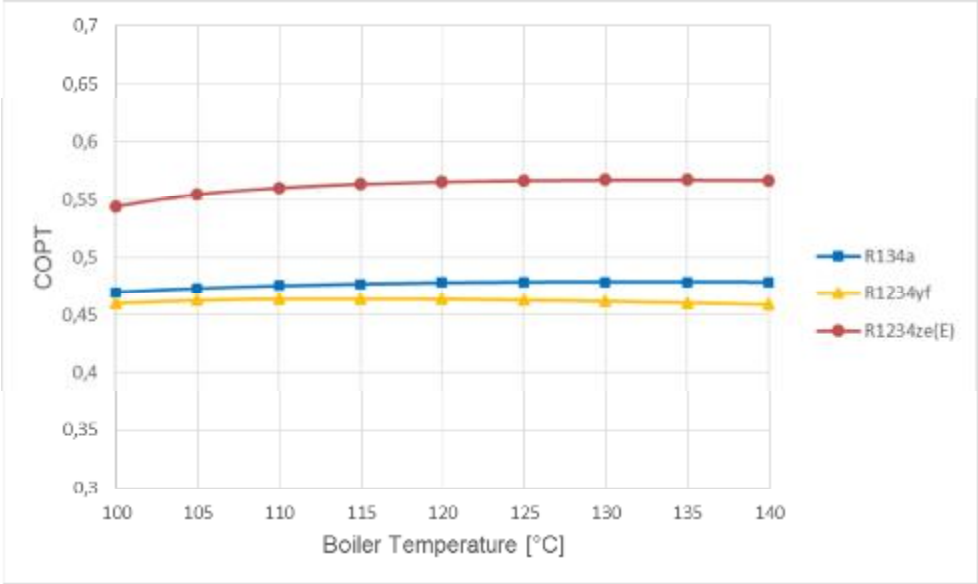

Figure 4.1. Variation of COPT with boiler temperature at T_{eva}:15 °C, T_{con}:45 °C, P_{boil}:30 bar and $\Delta T_{sub}=\Delta T_{sup}$=5 °C

In the figure given below, COPT value as a function of boiler temperature is illustrated. 15 °C evaporator temperature, 45 °C condenser temperature and 80 bar supercritical pressure are set as parameters. It is observed that, all these refrigerants have similar trends in the given temperature range. At small temperatures, all refrigerants have quite close COPT values. After a certain temperature, they diverge from each other. Additionally, raising boiler temperature has decremental effect on COPT value. Highest COPT values are 0.831, 0.774 and 0.861 for R134a, R1234yf and R1234ze(E), respectively. That is to say, R1234ze(E) has slightly higher COPT value than R134a, while R1234yf has the smallest COPT at high boiler temperature.

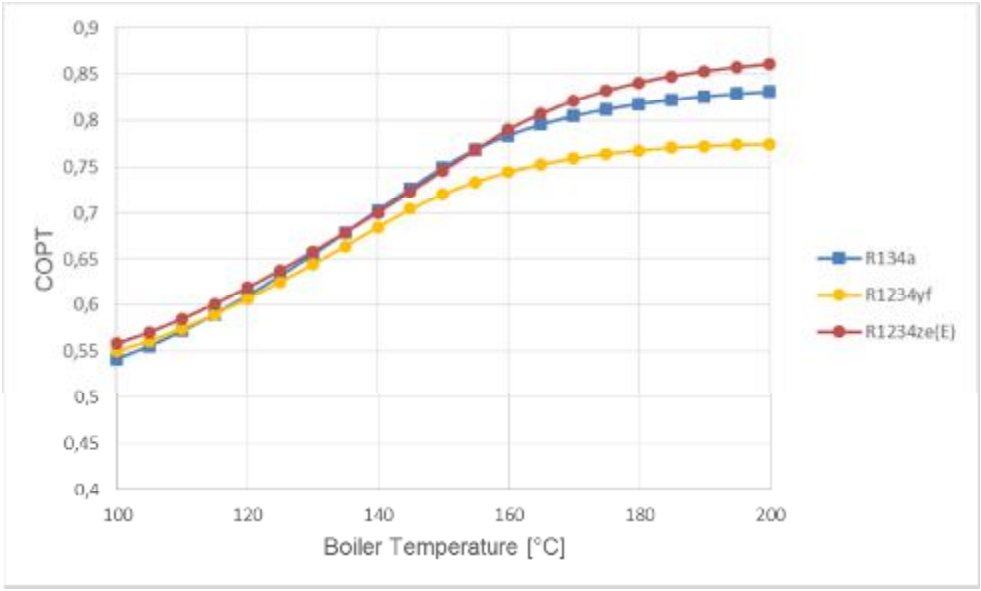

Figure 4.2. Variation of COPT with boiler temperature at T_{eva}:15 °C, T_{con}:45 °C, P_{boil}:80 bar and $\Delta T_{sub}=\Delta T_{sup}$=5 °C

Figures 4.3-5. exhibit the influence of boiler temperature on COPT at 30 bar subcritical boiler pressure, 15 °C evaporator, 45 °C condenser and 5 °C subcooling/superheating temperature. As expected, COPT values increase with increasing efficiencies. Each refrigerant has an optimum COPT value in given boiler temperature range. Optimum temperatures of R134a and R1234ze(E) are reached in the range of 130-135 °C boiler temperature while optimum values are arrived at about 115 °C boiler temperature for R1234yf. Table 4.3. illustrates the highest efficiencies of each refrigerant. In addition, the results obtained for high values (HV) and low values (LV) are approximately 28% higher and 39% lower than those for medium values (MV) for these refrigerants.

Table 4.3. Maximum COPT values for different efficiencies at T_{eva}:15 °C, T_{con}:45 °C, P_{boil}:30 bar and $\Delta_{sub}=\Delta_{sup}$=5 °C

	R134a	R1234yf	R1234ze(E)
LV	0.345	0.333	0.480
MV	0.479	0.463	0.567
HV	0.615	0.598	0.731

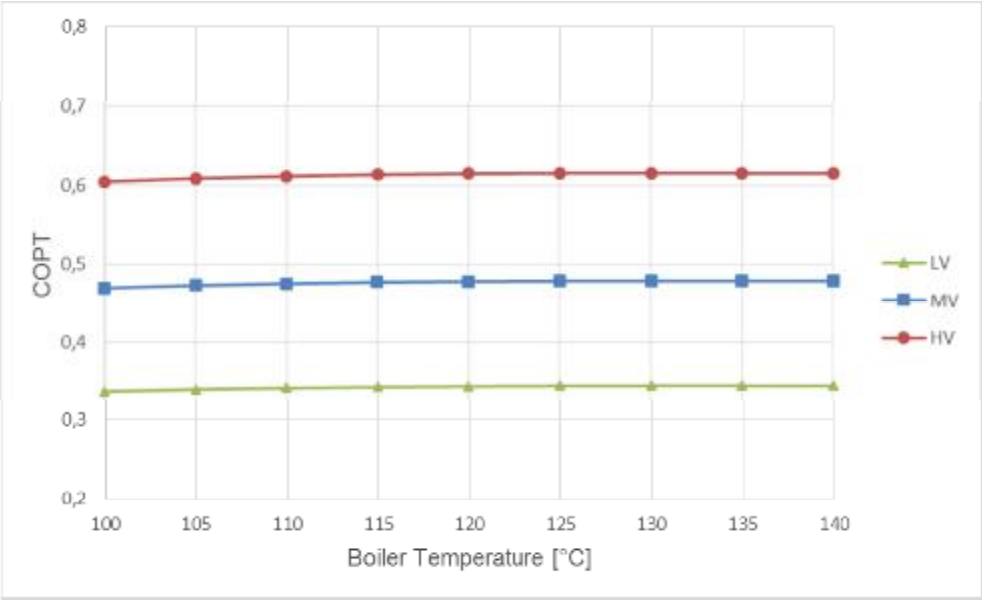

Figure 4.3. Variation of COPT with boiler temperature for different efficiencies at T_{eva}:15 °C, T_{con}:45 °C, P_{boil}:30 and $\Delta T_{sub}=\Delta T_{sup}$=5 °C bar for R134a

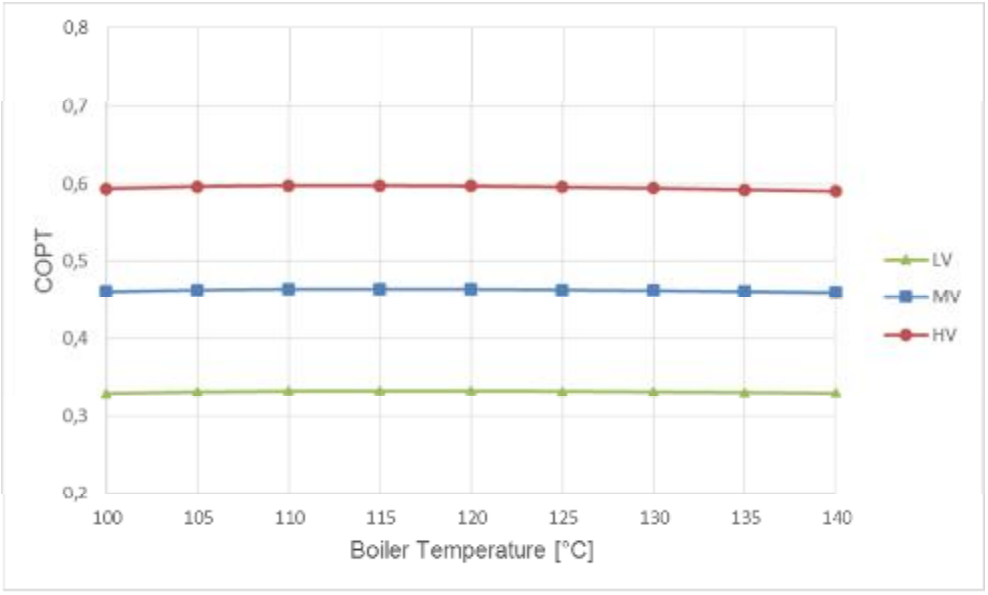

Figure 4.4. Variation of COPT with boiler temperature for different efficiencies at T_{eva}:15 °C, T_{con}:45 °C, P_{boil}:30 and $\Delta T_{sub}=\Delta T_{sup}$=5 °C bar for R1234yf

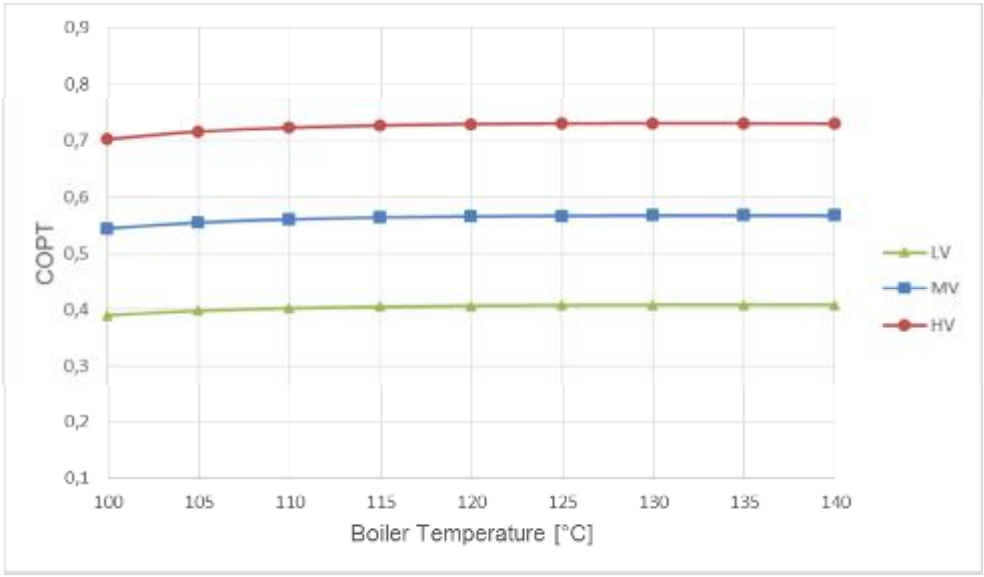

Figure 4.5. Variation of COPT with boiler temperature for different efficiencies at T_{eva}:15 °C, T_{con}:45 °C, P_{boil}:30 and $\Delta T_{sub}=\Delta T_{sup}$=5 °C bar for R1234ze(E)

COPT values as a function of boiler temperature at 80 bar supercritical pressure is demonstrated in figures 4.6-4.8. Parameters are considered as system component efficiencies, namely LV, MV and HV. Simulation is carried out at 15 °C evaporator, 45 °C condenser and 5 °C subcooling/superheating temperature. In order to prevent the decomposition of refrigerants, boiler temperature is limited to 200 °C. It is observe that, all these refrigerants show similar trends against increasing component efficiencies. Beyond a certain temperature, increment of all curves are slowed down and they converge to an optimum point. Table 4.4. exhibits the maximum COPT values obtained at 200 °C boiler temperature. It is seen from figures that, percent effect of efficiencies are reduces with increasing boiler temperature. At the top boiler temperature, the results obtained for high values (HV) and low values (LV) are approximately 30% higher and 41% lower than those for medium values (MV) for these refrigerants.

It can be inferred that, component efficiencies at supercritical pressures are more effective parameters than those at subcritical pressures. In other words, component efficiencies makes higher percent increment of COPT value for these refrigerants at supercritical pressures.

Table 4.4. Maximum COPT values for different efficiencies at T_{eva}:15 °C, T_{con}:45 °C, P_{boil}:80 bar and $\Delta T_{sub}=\Delta T_{sup}$=5 °C

	R134a	R1234yf	R1234ze(E)
LV	0.588	0.545	0.607
MV	0.831	0.775	0.861
HV	1.084	1.015	1.127

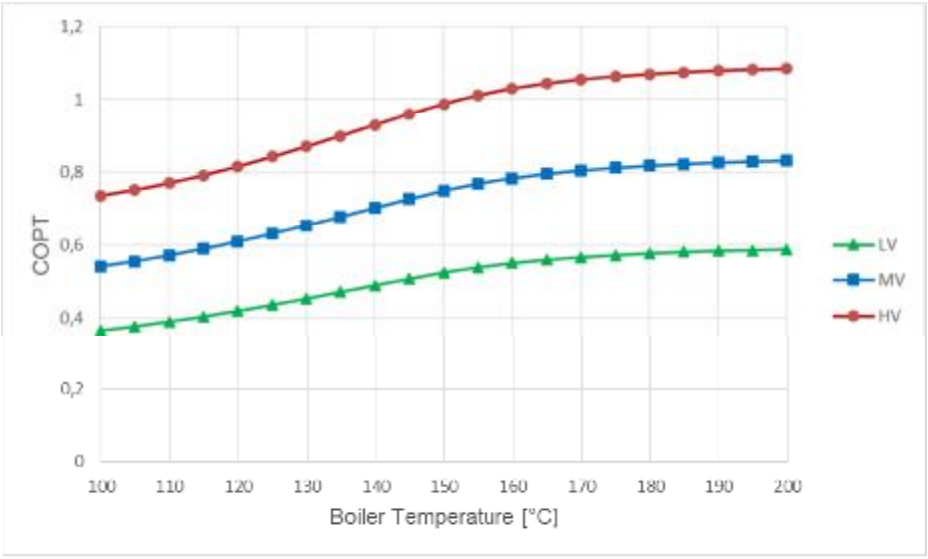

Figure 4.6. Variation of COPT with boiler temperature for different efficiencies at T_{eva}:15 °C, T_{con}:45 °C, P_{boil}:80 bar and $\Delta T_{sub}=\Delta T_{sup}$=5 °C for R134a

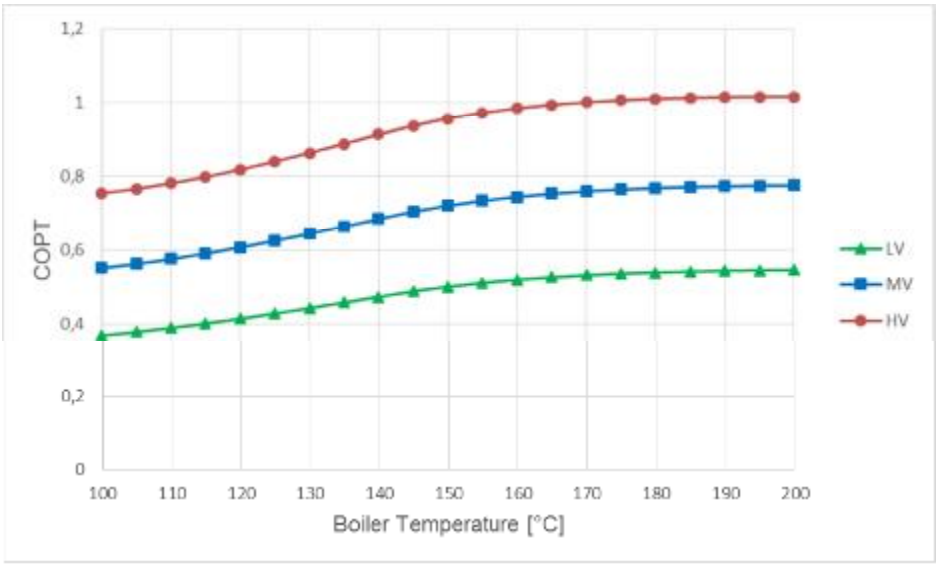

Figure 4.7. Variation of COPT with boiler temperature for different efficiencies at T_{eva}:15 °C, T_{con}:45 °C, P_{boil}:80 bar and $\Delta T_{sub}=\Delta T_{sup}$=5 °C for R1234yf

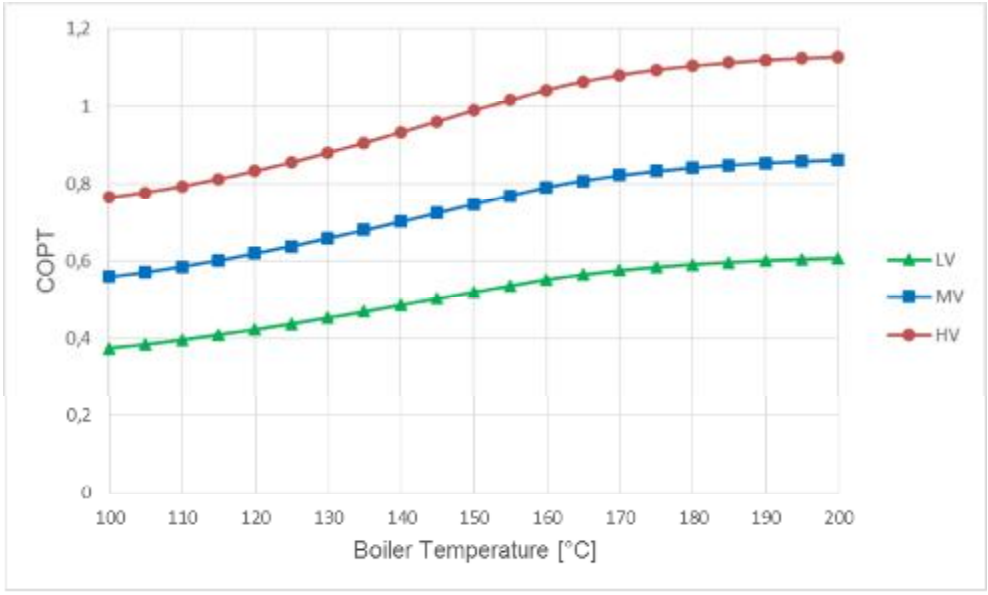

Figure 4.8. Variation of COPT with boiler temperature for different efficiencies at T_{eva}:15 °C, T_{con}:45 °C, P_{boil}:80 bar and $\Delta T_{sub}=\Delta T_{sup}$=5 °C for R1234ze(E)

4.3. Effect of Evaporation and Condensation Temperatures on total cooling performance (COPT)

4.3.1. Low Temperature Heat Source Condition

4.3.1.1. Low Pressure Condition

Figure 4.9. shows COPT as a function of evaporation and condensation temperatures at 100 °C boiler temperature and subcritical pressure of 30 bar while both superheating and subcooling temperature differences are 5 °C. Minimum values of COPT for R134a, R1234yf and R1234ze(E) are 0.125, 0.120 and 0.161, respectively. Maximum values of COPT for R134a, R1234yf and R1234ze(E) are 0.469, 0.46 and 0.544, respectively. For this boiler pressure and temperature condition, R1234ze(E) gives the highest and R1234yf gives the lowest COPT value. COPT difference of R134a and R1234yf changes between 1.09% and 3.91% while

that of R1234ze(E) and R134a changes between 15.15% and 30.21%. In addition, COPT values of all three working fluids increase with the increase in evaporation temperature and increase with the decrease in condensation temperature.

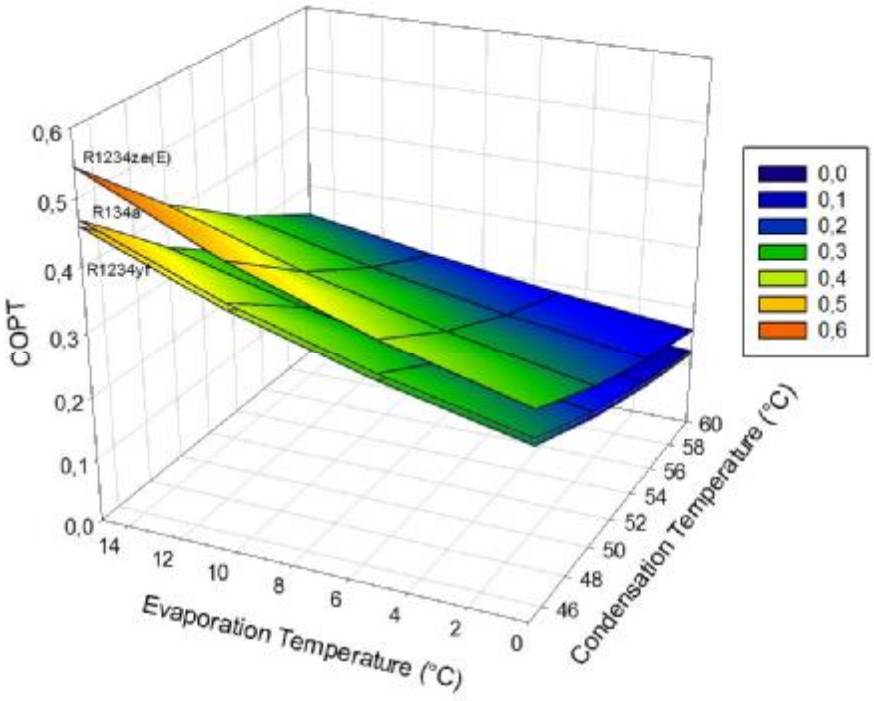

Figure 4.9. Variation of COPT with evaporation and condensation temperatures at T_{boil}:100 °C, P_{boil}:30 bar and $\Delta T_{sub}=\Delta T_{sup}=$ 5 °C

4.3.1.2. High Pressure Condition

Figure 4.10. illustrates the variation of COPT with evaporation and condensation temperatures at supercritical pressure of 80 bars while both superheating and subcooling temperature differences are 5 °C. Lowest values of COPT for R134a, R1234yf and R1234ze(E) are 0.198, 0.194 and 0.205 respectively. Highest values of COPT for R134a, R1234yf and

R1234ze(E) are 0.547, 0.546 and 0.560, respectively. It is seen that all three surface are rather close to each other. For this boiler pressure and boiler temperature condition, R1234ze(E) gives the highest COPT value, but it is not possible to say that R134a has greater COPT value than R1234yf for all points. On the contrary, R1234yf has greater value than R134a at most of the points, which has a difference up to 1.51%. COPT difference of R1234ze(E) and R134a changes between 4.62% and 2.34% . It is demonstrated that COP values for all these working fluids increases with increase in evaporator temperature, While they decrease with the increase in condensation temperature.

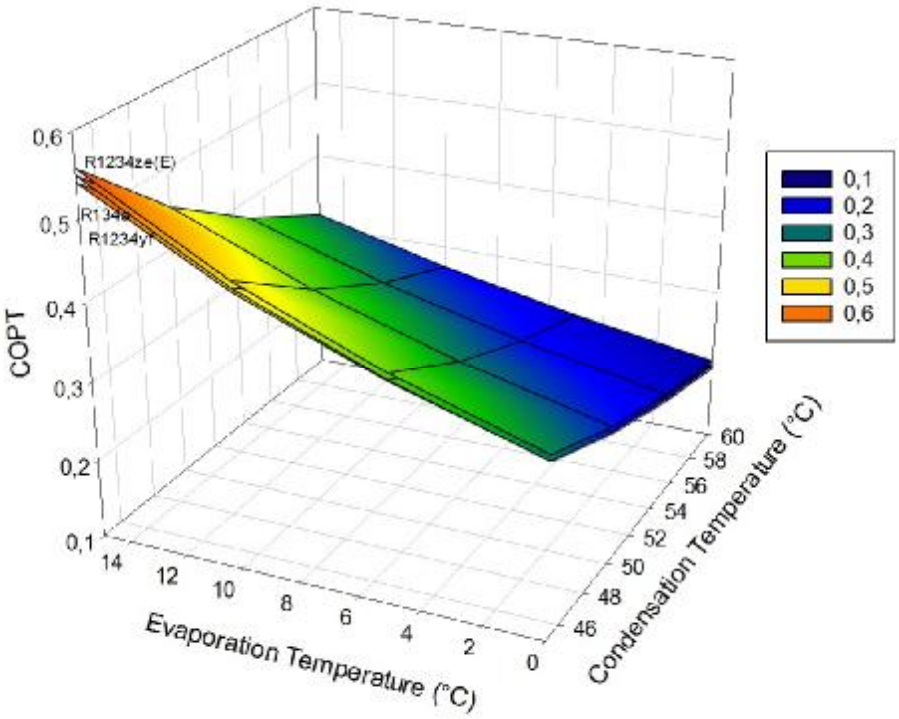

Figure 4.10. Variation of COPT with evaporation and condensation temperatures at T_{boil}:100 °C, P_{boil}:80 bar and $\Delta T_{sub}=\Delta TT_{sup}=$ 5 °C

4.3.2. Medium Temperature Heat Source Condition

4.3.2.1. Low Pressure Condition

Figure 4.11. exhibits COPT according to evaporation and condensation temperatures while both superheating and subcooling temperature differences are 5 °C. Minimum values of COPT for R134a, R1234yf and R1234ze(E) are 0.126, 0.118 and 0.167, respectively. Maximum values of COPT for R134a, R1234yf and R1234ze(E) are 0.478, 0.458 and 0.567, respectively. For this boiler pressure and boiler temperature condition, R1234ze(E) gives the highest and R1234yf gives the lowest COPT value. COPT difference of R134a and R1234yf changes between 3.48% and 6.07% while that of R1234ze(E) and R134a changes between 17.70% and 33.81%. It is also observed that, increase in evaporation temperature and decrease in condenser temperature leads to increase in COPT for all these working fluids.

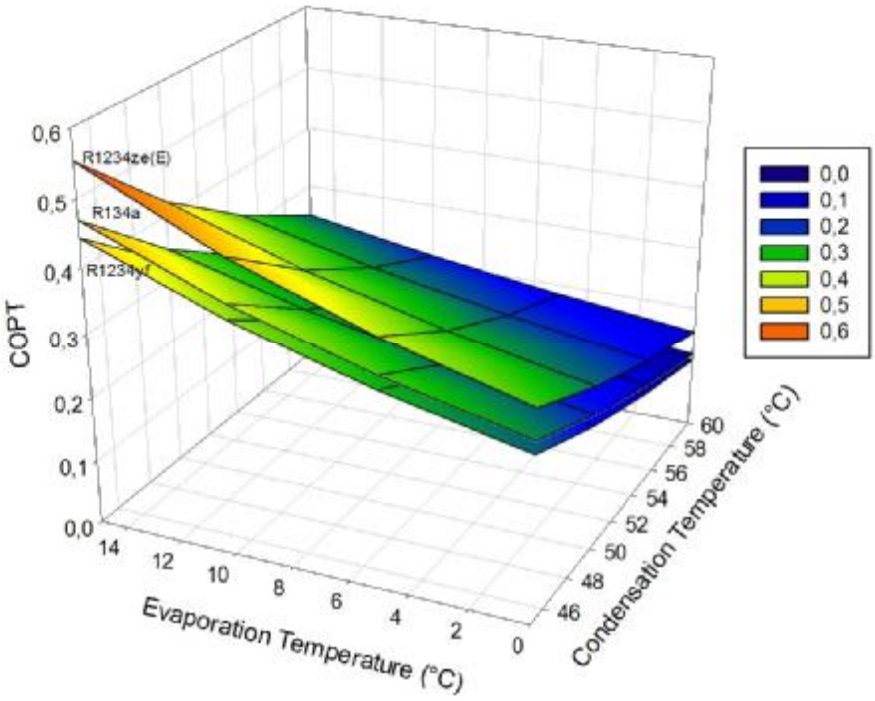

Figure 4.11. Variation of COPT with evaporation and condensation temperatures at T_{boil}:140 °C, P_{boil}:30 bar and $\Delta T_{sub}=\Delta T_{sup}=$ 5 °C

4.3.2.2. High Pressure Condition

Figure 4.12. demonstrates COPT as a function of evaporation and condensation temperatures while both superheating and subcooling temperature differences are 5 °C. Peak values of COPT for R134a, R1234yf and R1234ze(E) are 0.242, 0.226 and 0.241, respectively. Lowest values of COPT for R134a, R1234yf and R1234ze(E) are 0.703, 0.685 and 0.700, respectively. For this boiler pressure and boiler temperature condition, R134a gives highest (exceptionally, R1234ze(E) has slightly higher COPT value than R134a in the small region of high evaporation temperature) and R1234yf gives the lowest COPT values. COPT difference of R134a and

R1234yf changes between 2.61% and 6.81% while that of R1234ze(E) and R134a changes between -0.54% and 1.01%. Effect of evaporation temperature decreases with increasing condensation temperature for all three working fluids.

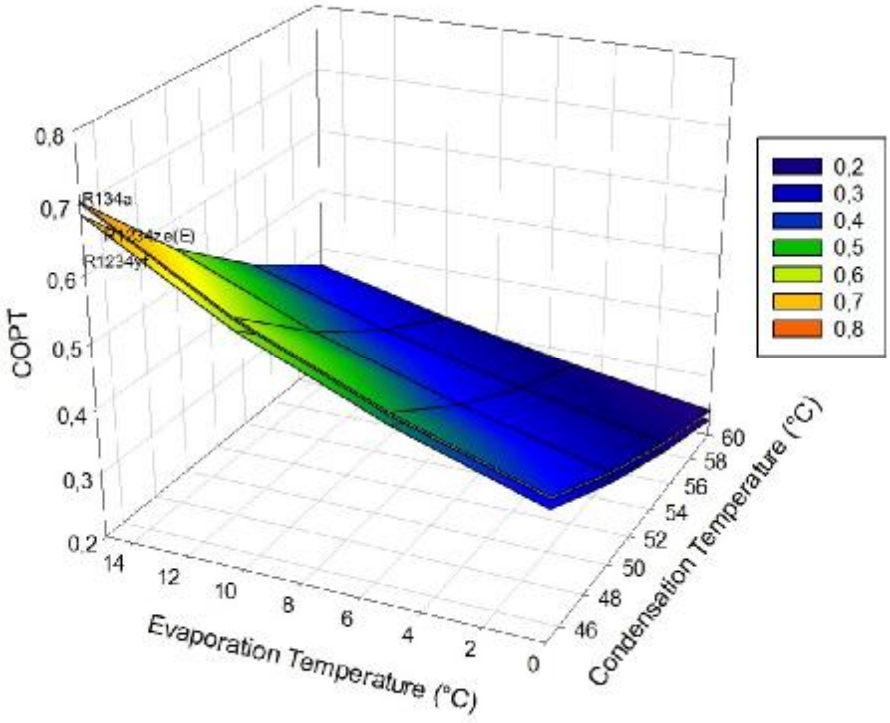

Figure 4.12. Variation of COPT with evaporation and condensation temperatures at T_{boil}:140 °C, P_{boil}:80 bar and $\Delta T_{sub}=\Delta T_{sup}=$ 5 °C

4.3.3. High Temperature Heat Source Condition

4.3.3.1. Low Pressure Condition

Figure 4.13. displays the variation of COPT with evaporation and condensation temperatures while both superheating and subcooling temperature

differences are 5 °C. According to the figure, lowest values of COPT for R134a, R1234yf and R1234ze(E) are 0.122, 0.112 and 0.162, respectively. Highest values of COPT for R134a, R1234yf and R1234ze(E) are 0.471, 0.443 and 0.557, respectively. For this boiler pressure and boiler temperature condition, R1234ze(E) gives the highest and R1234yf gives the lowest COPT value. COPT difference of R134a and R1234yf changes between 5.45% and 7.98% while that of R1234ze(E) and R134a changes between 17.54% and 33.83%. Effect of evaporation temperature on COPT decreases with increasing condensation temperature for all working fluids. Additionally, COPT values for all these working fluids increases as evaporation temperature rises, and decreases as condensation temperature rises.

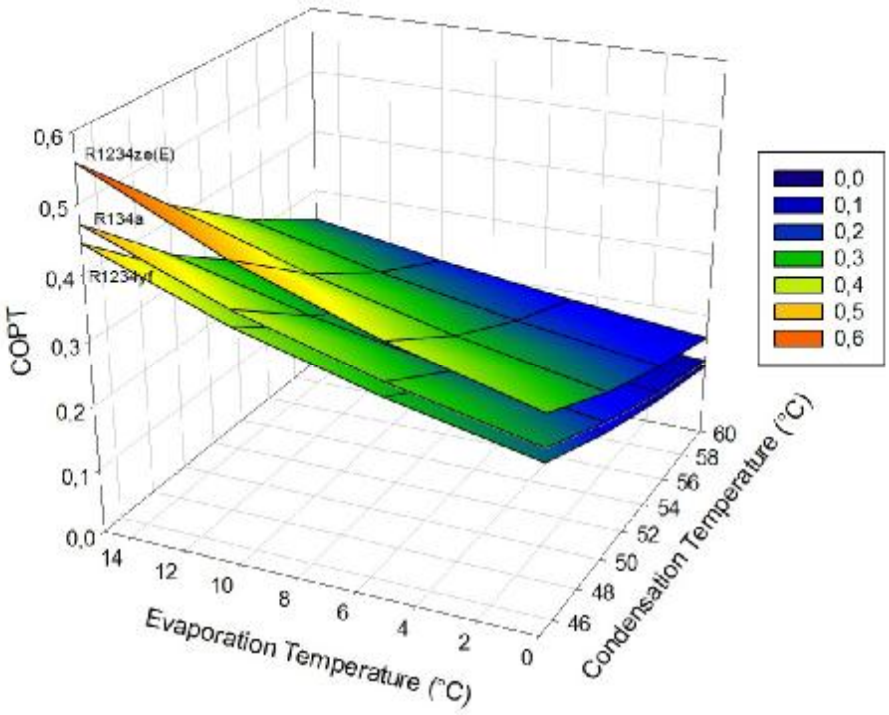

Figure 4.13. Variation of COPT with evaporation and condensation temperatures at T_{boil}: 180 °C, P_{boil}: 30 bar and $\Delta T_{sub}=\Delta T_{sup}=$ 5 °C

4.3.3.2. High Pressure Condition

Figure 4.14. shows COPT as a function of evaporation and condensation temperatures while both superheating and subcooling temperature differences are 5 °C. Lowest values of COPT for R134a, R1234yf and R1234ze(E) are 0.280, 0.251 and 0.280, respectively. Peak values of COPT for R134a, R1234yf and R1234ze(E) are 0.818, 0.767 and 0.841, respectively. For this boiler pressure and boiler temperature condition, R1234ze(E) gives the highest and R1234yf gives the smallest COPT value. COPT difference of R134a and R1234yf changes between 6.12% and 10.43% while that of R1234ze(E) and R134a changes between 2.11% and 4.39%. Effect of evaporation temperature on COPT decreases with increasing condensation temperature for all working fluids. It also seen that, when the evaporator temperature increases COPT value increases; however, when the condenser temperature increases COPT value decreases for all these working fluids.

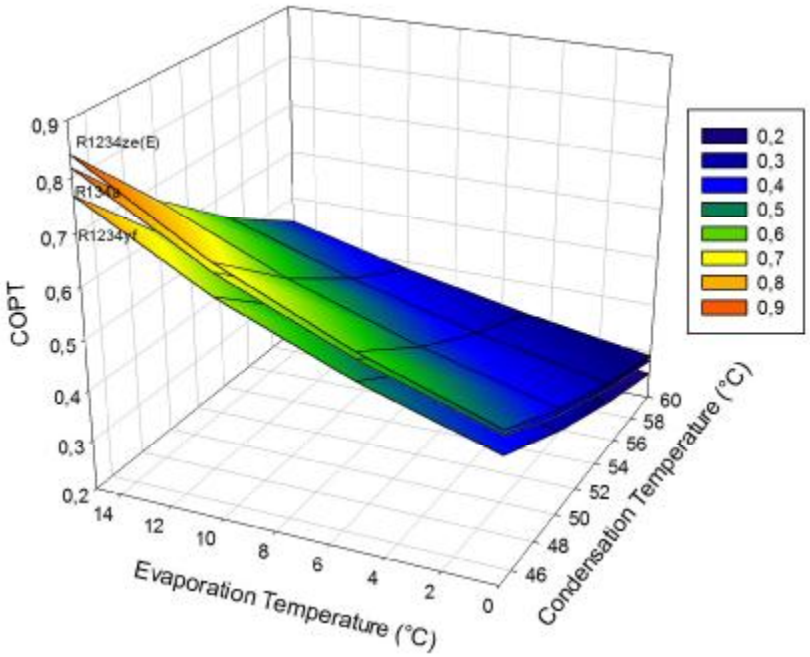

Figure 4.14. Variation of COPT with evaporation and condensation temperatures at T_{boil}: 140 °C, P_{boil}: 80 and $\Delta T_{sub}=\Delta T_{sup}$=5 °C bar

4.4. Effect of Subcooling and Superheating Temperatures on total cooling performance (COPT)

In the following section, influence of subcooling and superheating temperature differences at the end of the condenser and evaporator are examined. For the subcritical region, 140 °C boiler temperature and 30 bar boiler pressure are set while the evaporator and condenser temperatures are 15 °C and 45 °C. Figures 4.15-17. demonstrate the variation of COPT with subcooling and superheating temperatures using MV efficiencies. It is observed that, COPT values for all these working fluids slightly increase with the increase in subcooling and superheating temperatures. Lowest COPT values are 0.467, 0.444 and 0.553 for R134a, R1234yf and R1234ze(E), respectively. Highest COPT values are 0.478,

0.458 and 0.567 for R134a, R1234yf and R1234ze(E), respectively. In other words, R1234yf showed the highest and R134a showed the lowest increment of COPT.

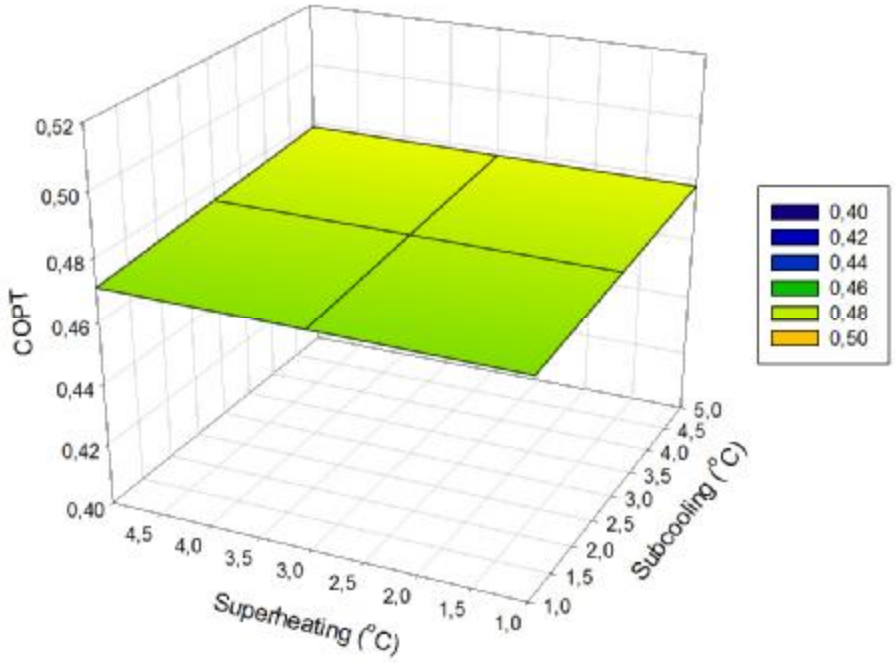

Figure 4.15. Variation of COPT with subcooling and superheating temperatures at T_{boil}:140 °C, P_{boil}:30 bar for R134a

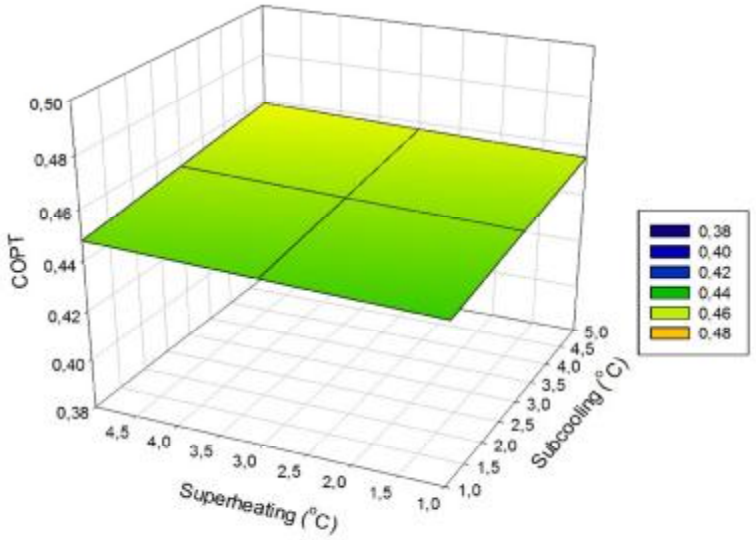

Figure 4.16. Variation of COPT with subcooling and superheating temperatures at T_{boil}: 140 °C, P_{boil}: 30 bar for R1234yf

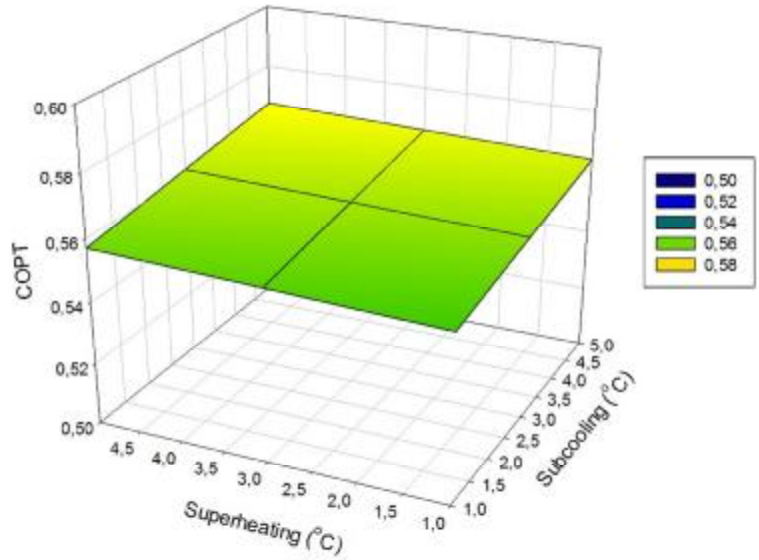

Figure 4.17. Variation of COPT with subcooling and superheating temperatures at T_{boil}: 140 °C, P_{boil}: 30 bar for R1234ze(E)

Figures 4.18-20. exhibit COPT as a function of subcooling and superheating temperatures at 80 bar supercritical boiler pressure, 180 °C boiler temperature using MV efficiencies. It is seen that, COPT values for all these working fluids increases with elevating subcooling and superheating temperatures. Lowest COPT values are 0.467, 0.444 and 0.553 for R134a, R1234yf and R1234ze(E), respectively. Highest COPT values are 0.478, 0.458 and 0.567 for R134a, R1234yf and R1234ze(E), respectively. That is, COPT value R1234yf is showed the highest reaction as that of R134a showed the smallest reaction to change in subcooling and superheating temperatures. It is also observed that, subcooling and superheating temperatures has similar effect on COPT.

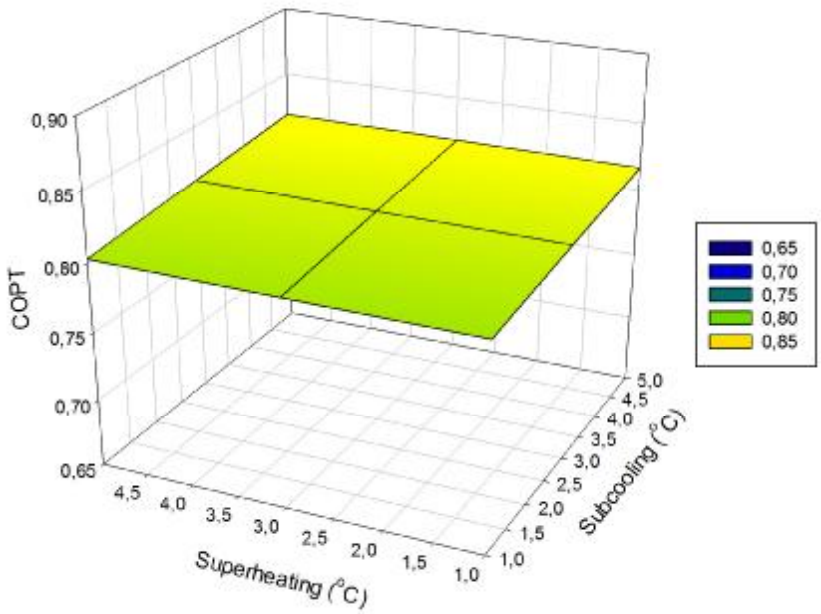

Figure 4.18. Variation of COPT with subcooling and superheating temperatures at T_{boil}: 180 °C, P_{boil}: 80 bar for R134a

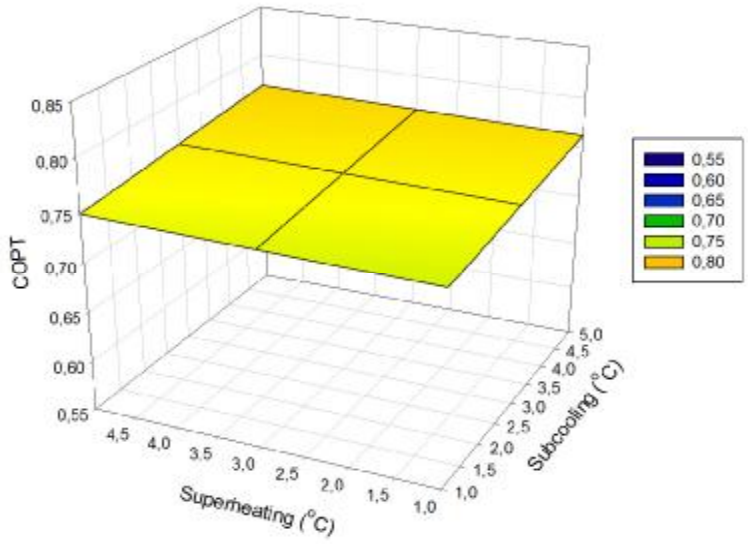

Figure 4.19. Variation of COPT with subcooling and superheating temperatures at T_{boil}: 180 °C, P_{boil}: 80 bar for R1234yf

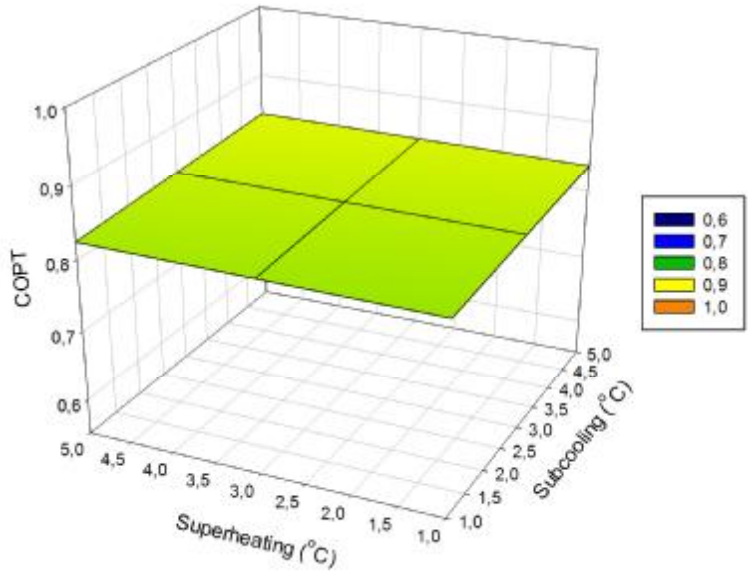

Figure 4.20. Variation of COPT with subcooling and superheating temperatures at T_{boil}: 180 °C, P_{boil}: 80 bar for R1234ze(E)

Figures 4.21-23. illustrate COPT versus subcooling and superheating temperatures at 30 bar subcritical boiler pressure for different efficiency values of system components. Simulation is carried out at 15 °C evaporator, 45 °C condenser temperature and 140 °C boiler temperature. It is clear that higher efficiency gives higher COPT value. For subcritical pressures, COPT values obtained for high values (HV) and low values (LV) are approximately 28% higher and 39% lower than those for medium values (MV) for these refrigerants. In addition, maximum COPT values of R134a, R1234yf and R1234ze(E) are calculated as 0.615, 0.590 and 0.73, respectively.

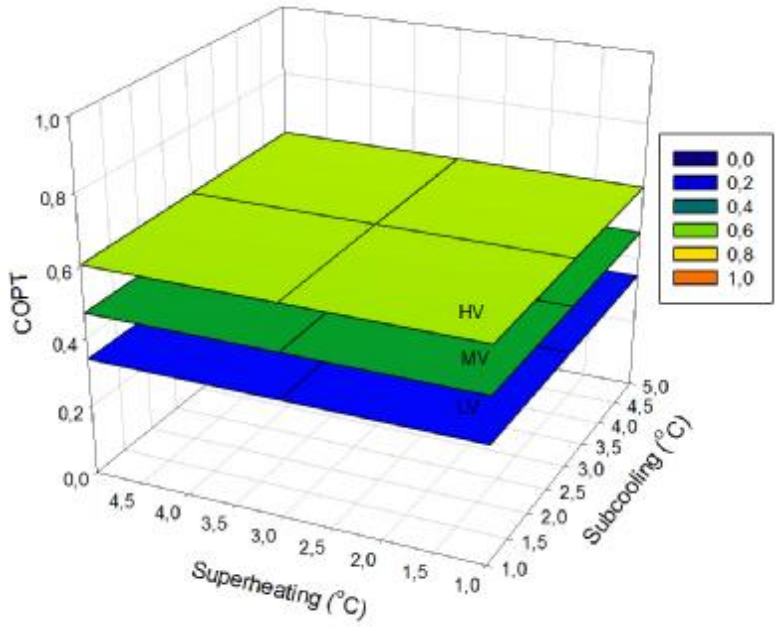

Figure 4.21. Variation of COPT with subcooling and superheating temperatures for different efficiencies at T_{boil}:140 °C and P_{boil}:30 bar for R134a

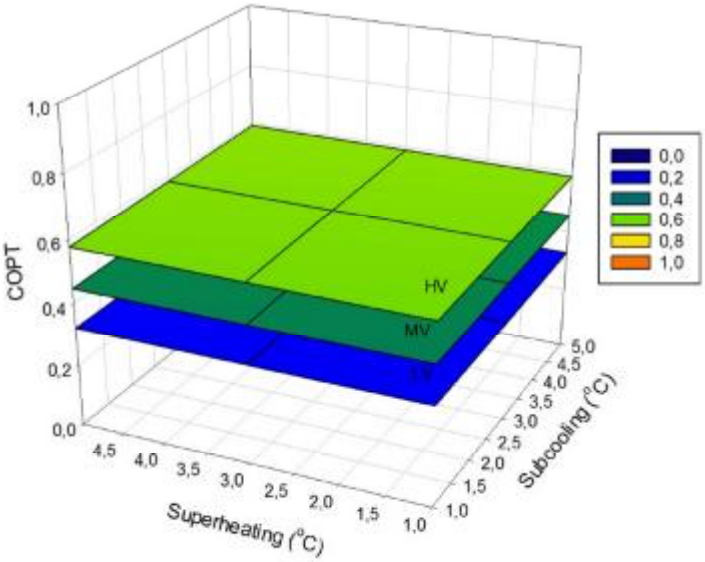

Figure 4.22. Variation of COPT with subcooling and superheating temperatures for different efficiencies at T_{boil}:140 °C and P_{boil}:30 bar for R1234yf

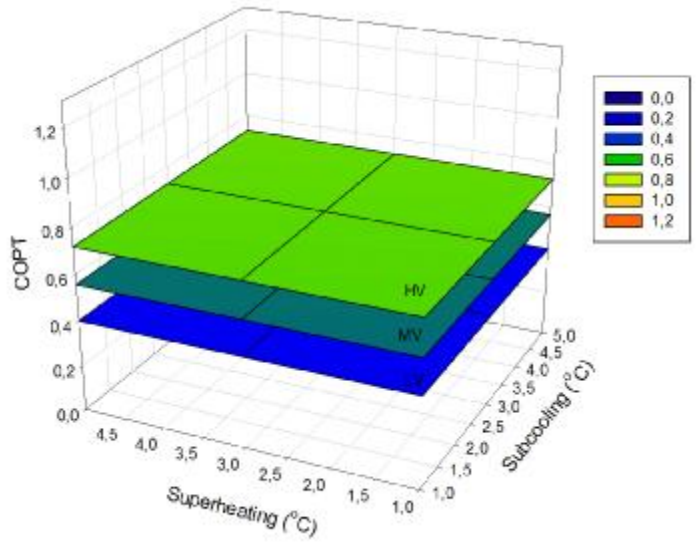

Figure 4.23. Variation of COPT with subcooling and superheating temperatures for different efficiencies at T_{boil}:140 °C and P_{boil}:30 bar for R1234ze(E)

Variation of COPT with subcooling and superheating temperature for different efficiencies at 80 bar supercritical pressure are demonstrated in figures 4.24-26. Simulation is executed at 15 °C evaporator, 45 °C condenser and 180 °C boiler temperature. COPT values, which are determined for high values (HV) and low values (LV), are approximately 31% higher and 41% lower than those values determined for medium values (MV) for these refrigerants at supercritical pressures. It is seen that, maximum COPT values of R134a, R1234yf and R1234ze(E) are determined as 1.07, 1.01 and 1.1, respectively.

It can be inferred that, component efficiencies at supercritical pressures are more effective parameters than those at subcritical pressures. In other words, component efficiencies makes higher percent increment of COPT value for the corresponding refrigerants at supercritical pressures.

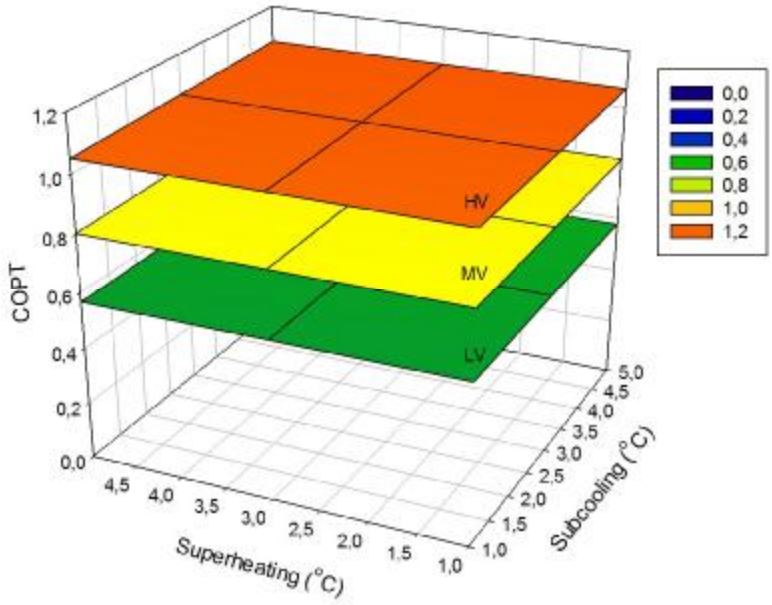

Figure 4.24. Variation of COPT with subcooling and superheating temperatures for different efficiencies at T_{boil}:180 °C and P_{boil}:80 bar for R134a

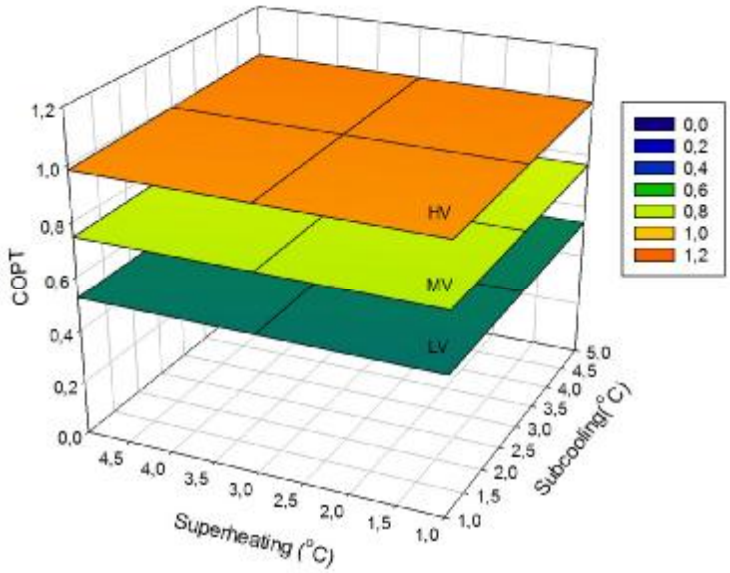

Figure 4.25. Variation of COPT with subcooling and superheating temperatures for different efficiencies at T_{boil}:180 °C and P_{boil}:80 bar for R1234yf

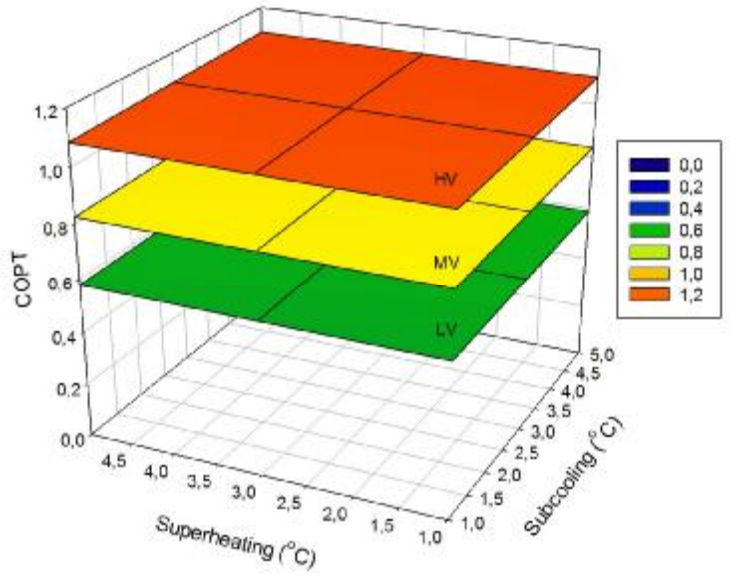

Figure 4.26. Variation of COPT with subcooling and superheating temperatures for different efficiencies at T_{boil}:180 °C and P_{boil}:80 bar for R1234ze(E)

4.5. Effect of System Component Efficiencies on total cooling performance (COPT)

Figures 4.27-29. demonstrate the influence of evaporation and condensation temperature at 80 bar boiler pressure, 180 °C boiler temperature and 5 °C subcooling/superheating temperature. As expected, COPT values increase with increasing component efficiencies. The results obtained for high values (HV) and low values (LV) are roughly 32% higher and 42% lower than those for medium values (MV) for all these working fluids. Highest COPT values are 0.562, 0.801 and 1.049 for LV, MV and HV for R134a, respectively. Highest COPT values are 0.518, 0.740 and 0,974 for LV, MV and HV for R1234yf. Highest COPT values are 0.575, 0.820 and 1.077 for LV, MV and HV for R1234ze(E).

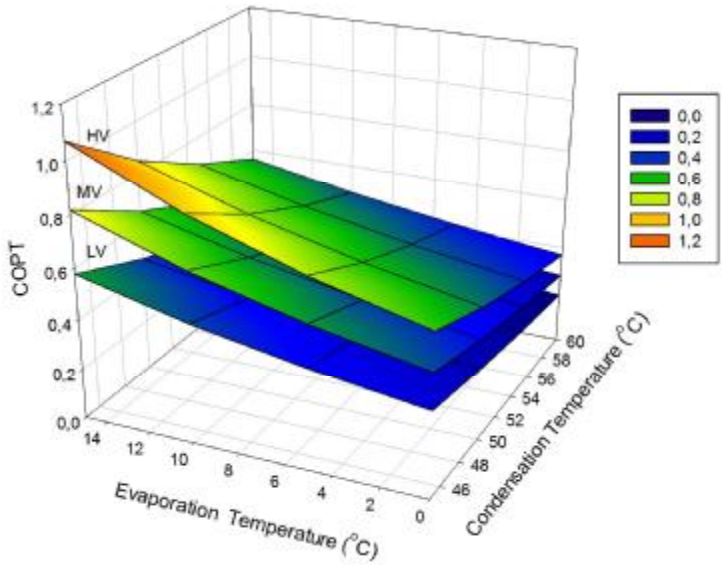

Figure 4.27. Variation of COPT with T_{eva} and T_{con} for different efficiencies using R134a

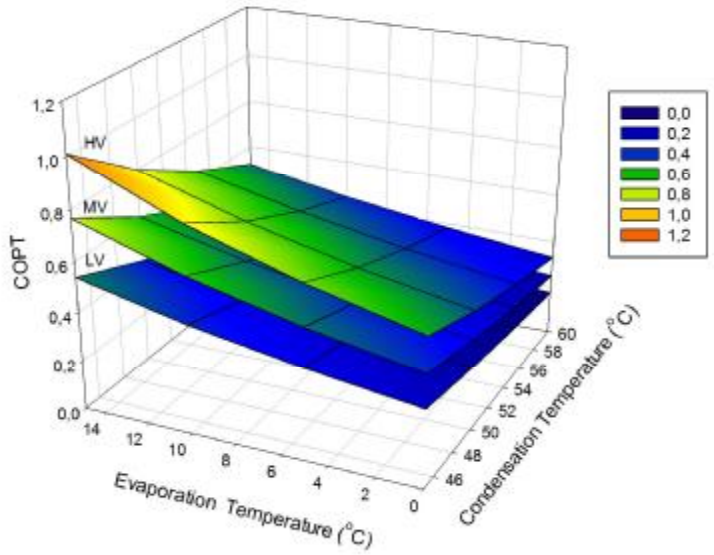

Figure 4.28. Variation of COPT with T_{eva} and T_{con} for different efficiencies using R1234yf

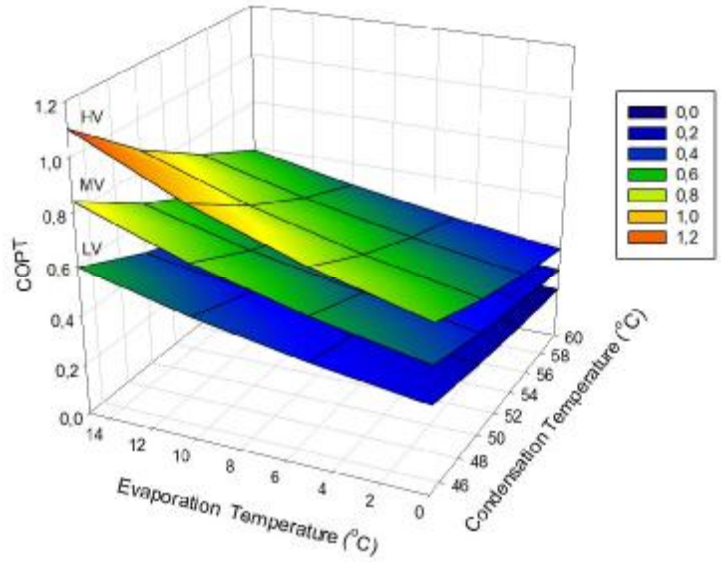

Figure 4.29. Variation of COPT with T_{eva} and T_{con} for different efficiencies using R1234ze(E)

4.6. Effect of Evaporation and Condensation Temperatures on COPH

Figure 4.30. exhibits COPH as a function of evaporation and condensation temperatures at 100 °C and subcooling pressure (30 bar) while both superheating and subcooling temperature differences are 1 °C. Minimum values of COPH for R134a, R1234yf and R1234ze(E) are 0.126, 0.120 and 0.165, respectively. Maximum values of COPH for R134a, R1234yf and R1234ze(E) are 0.482, 0.472 and 0.565. For this boiler pressure and boiler temperature condition, R1234ze(E) gives highest the and R1234yf gives the lowest COPH value. COPH difference of R134a and R1234yf changes between 1.64% and 4.81% while that of R1234ze(E) and R134a changes between 16.21% and 32,13%. Effect of evaporation temperature on COPH decreases with increasing condensation temperature for all three working fluids.

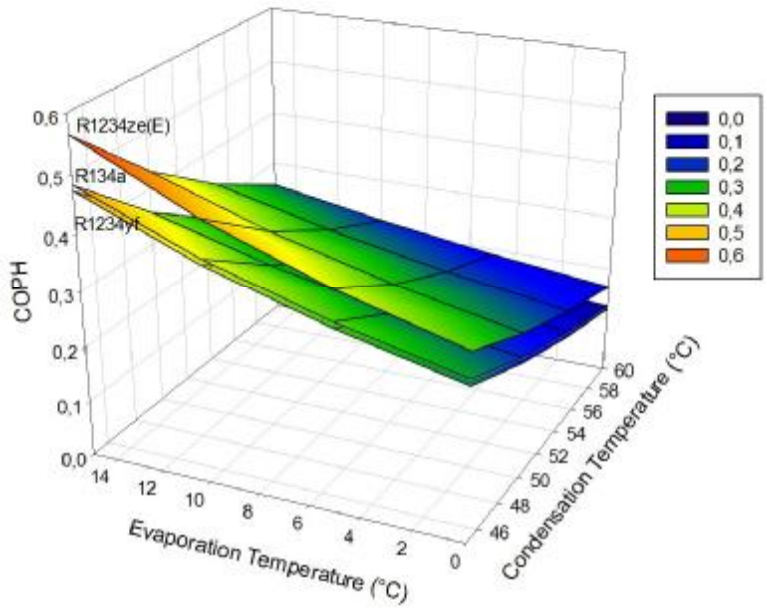

Figure 4.30. Variation of COPH with evaporation and condensation temperatures at T_{boil}: 100 °C, P_{boil}: 30 bar and $\Delta T_{sub}=\Delta T_{sup}=$ 1 °C

Figure 4.31. exhibits COPH as a function of evaporation and condensation temperatures while both superheating and subcooling temperature differences are 5 °C. Minimum values of COPH for R134a, R1234yf and R1234ze(E) are 0.313, 0.288 and 0.330, respectively. Maximum values of COPH for R134a, R1234yf and R1234ze(E) are 0.907, 0.870 and 0.947, respectively. For this boiler pressure and boiler temperature condition, R1234ze(E) gives the highest and R1234yf gives the lowest COPH value. COPH difference of R134a and R1234yf changes between 4.07% and 8.16% while that of R1234ze(E) and R134a changes between 3.71% and 6.39%. Effect of evaporation temperature on COPH decreases with increasing condensation temperature for all working fluids.

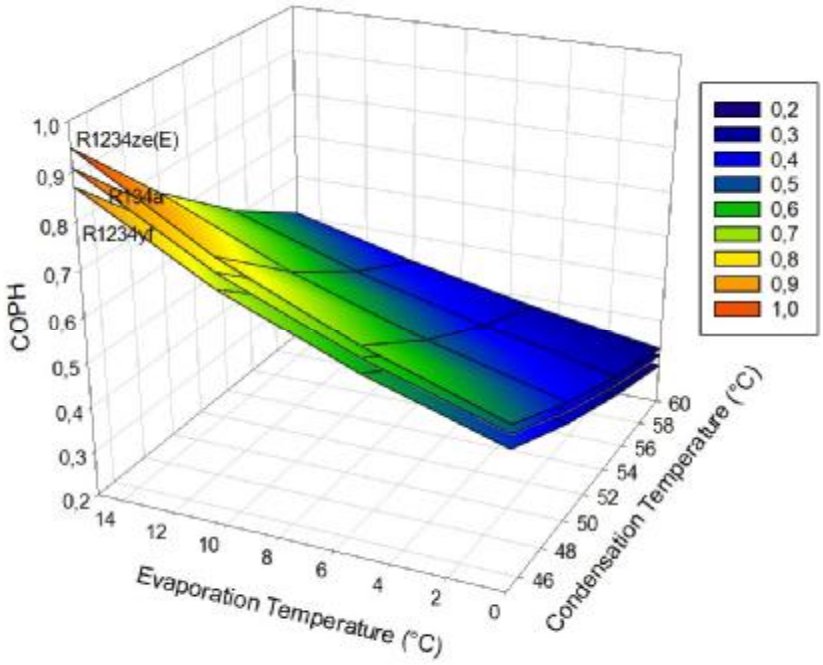

Figure 4.31. Variation of COPH with evaporation and condensation temperatures at T_{boil}: 180 °C, P_{boil}: 80 bar and $\Delta T_{sub}=\Delta T_{sup}=$ 5 °C

4.7. Effect of Evaporation and Condensation Temperatures on COPW

Parameters are selected in such a way that highest and lowest limit of the COPW could be observed. Figure 4.32. exhibits COPW as a function of evaporation and condensation temperatures at 100°C boiler temperature and 30 bar subcritical pressure while both superheating and subcooling temperature differences are 1 °C. Minimum values of COPW for R134a, R1234yf and R1234ze(E) are 12.1, 8.24 and 10.21, respectively. Maximum values of COPW for R134a, R1234yf and R1234ze(E) are 40.09, 29.75 and 34.62. For this boiler pressure and boiler temperature condition, unlike COPT performance, R134a gives the highest and R1234yf gives the lowest COPW value. COPW difference of R134a and R1234yf changes between 35.79% and 31.87% while that of R1234ze(E) and R134a changes between 13.64% and 15.61%. Additionally, COPW values increase with increasing evaporation temperature and decrease with increasing condensation temperature.

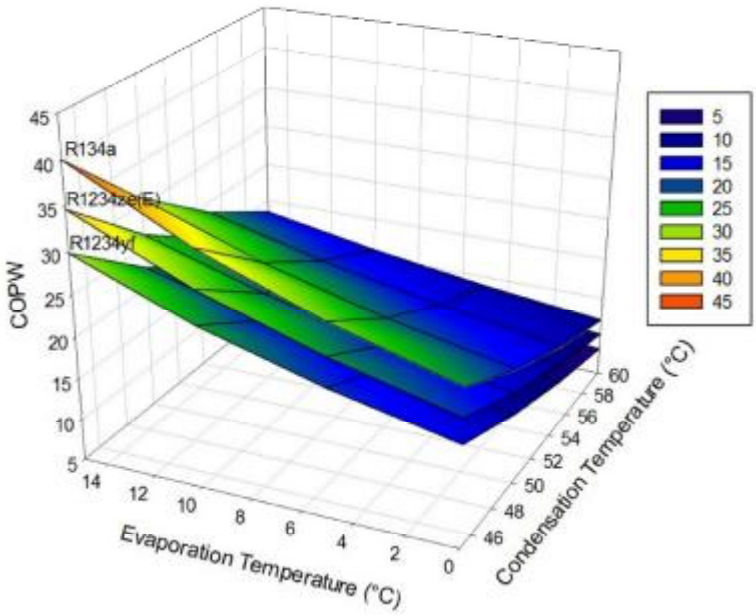

Figure 4.32. Variation of COPW with evaporation and condensation temperatures at T_{boil}: 100 °C, P_{boil}: 30 bar and $\Delta T_{sub}=\Delta T_{sup}=$ 1 °C

Figure 4.33. exhibits COPW versus evaporation and condensation temperatures while both superheating and subcooling temperature differences are 5 °C. Lowest values of COPW for R134a, R1234yf and R1234ze(E) are 8.88, 6.57 and 7.91, respectively. Peak values of COPH for R134a, R1234yf and R1234ze(E) are 27.62, 21.71 and 24.87, respectively. R134a gives the highest and R1234yf gives the lowest COPW value for this boiler pressure and boiler temperature condition. COPW difference of R134a and R1234yf changes between 21.39% and 26.01% while that of R1234ze(E) and R134a changes between 9.95% and 10.98%. Effect of evaporation temperature on COPW decreases with increasing condensation temperature for all working fluids.

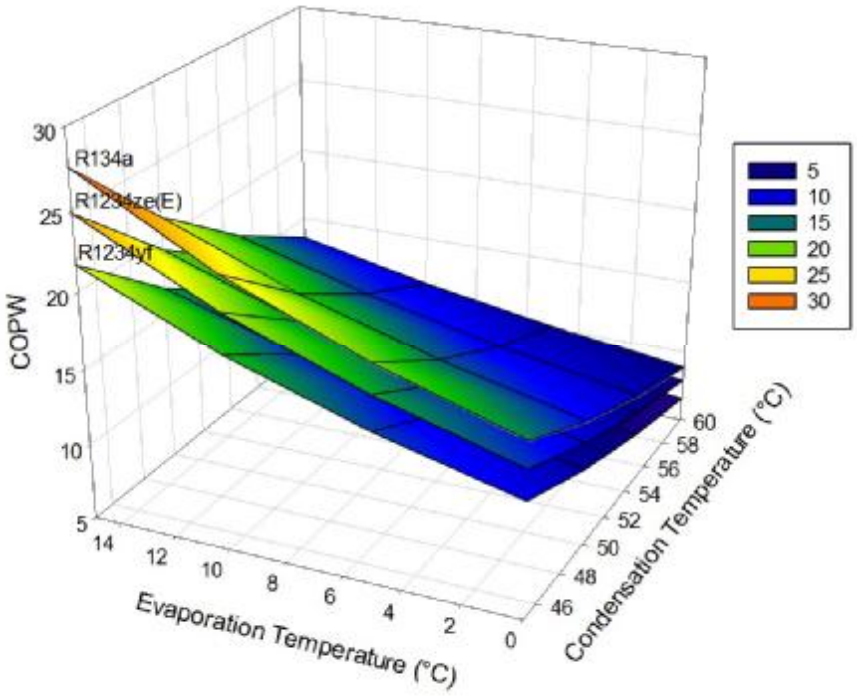

Figure 4.33. Variation of COPW with evaporation and condensation temperature at T_{boil}: 180 °C, P_{boil}: 80 bar and $\Delta T_{sub}=\Delta T_{sup}=$ 5 °C

5. CONCLUSIONS

In this thesis, transcritical organic Rankine vapor compression refrigeration system is studied using low GWP refrigerants with the utilization of ICE exhaust waste heat. Proposed low GWP refrigerants are R1234yf and R1234ze(E) which seen as alternatives to R134a. Both ORC and VCC system used same working fluid. Use of R1234ze(E) as the T-ORVC working fluid gives highest COPT for all analysed parameters. On the other hand, R1234yf shows slightly lower COPT value than R134a.

The influence of condenser, evaporator and boiler temperatures as well as refrigerant boiler pressure, system component efficiencies and subcooling/ superheating temperature differences are examined.

The results reveal that, COP values increase as boiler and evaporator temperature, boiler pressure, component efficiencies and subcooling/superheating temperature increases. However, COP values decreases as condenser temperature increases.

R1234ze(E) with the highest COPT value, shows much more decrease as condenser temperature increases above critical point. For subcritical pressures, COPT difference between R1234ze(E) and R134a varies between approximately 14% and 33%. However, maximum difference is roughly 4% at supercritical pressures.

Maximum COPT values are 1.084, 1.015 and 1.127 for R134a, R1234yf and R1234ze(E), respectively at 200 °C boiler temperature, 80 bar boiler pressure and HV efficiencies.

Obtained COPW values are very high in general. Thus, required electrical energy for the refrigerant pump is very low.

Study shows that both low GWP working fluids can be utilized as drop-in replacements to R134a which is a high GWP working fluid for the proposed refrigeration system.

REFERENCES

Abbas, L., Kim, S., and Schultz, K., 2016. Novel Reduced GWP Refrigerant Compositions To Replace R-134a in Stationary Air-conditioning and Refrigeration. International Refrigeration and Air Conditioning Conference.

Abed, H., Atashkari, K., Niazmehr, A., and Jamali, A., 2013. Thermodynamic optimization of combined power and refrigeration cycle using binary organic working fluid. International Journal of Refrigeration, 36(8):2160–2168.

Ahrens, C. D., 2003. Meteorology today : an introduction to weather, climate, and the environment. Cengage Learning, 624p.

Aneke, M., Agnew, B., Underwood, C., and Menkiti, M., 2012. Thermodynamic analysis of alternative refrigeration cycles driven from waste heat in a food processing application. International Journal of Refrigeration, 35(5):1349–1358.

Anonymous, 2008, Saving the Ozone Layer: Phasing Out Ozone Depleting Substances in Developing Countries, Paris.

Aphornratana, S., and Sriveerakul, T., 2010. Analysis of a combined Rankine-vapour-compression refrigeration cycle. Energy Conversion and Management, 51(12):2557–2564.

Armstead, J. R., and Miers, S. A., 2010. Review of Waste Heat Recovery Mechanisms for Internal Combustion Engines. Proceedings of the Asme Internal Combustion Engine Division Fall Technical Conference, 6:965–974.

Bennett, S., 2015. Heavy Duty Truck Systems. Mason, OH, Cengage Learning, Mason, OH Retrieved 368p.

Bolaji, B. O., and Huan, Z., 2013a. Ozone depletion and global warming: Case for the use of natural refrigerant. Renewable and Sustainable Energy Reviews, 18(1):49–54.

Bu, X. B., Li, H. S., and Wang, L. B., 2013. Performance analysis and working fluids selection of solar powered organic Rankine-vapor compression ice maker. Solar Energy, 95:271–278.

Calm, J. M., 2008. The next generation of refrigerants – Historical review, considerations, and outlook. International Journal of Refrigeration, 31(7):1123–1133.

Campana, F., Bianchi, M., Branchini, L., De Pascale, A., Peretto, A., Baresi, M., Vescovo, R., 2013. ORC waste heat recovery in European energy intensive industries: Energy and GHG savings. Energy Conversion and Management, 76:244–252.

Capata, R., and Toro, C., 2014. Feasibility analysis of a small-scale ORC energy recovery system for vehicular application. Energy Conversion and Management, 86:1078–1090.

Chen, H., Goswami, D. Y., and Stefanakos, E. K., 2010. A review of thermodynamic cycles and working fluids for the conversion of low-grade heat. Renewable and Sustainable Energy Reviews, 14(9):3059–3067.

Chiasson, A., 2016. Geothermal heat pump and heat engine systems: theory and practice. Wiley and Sons, 496p.

Cox, S., 2012. Losing Our Cool: Uncomfortable Truths About Our Air-Conditioned World. The New Press, 272p.

Demirkaya, G., and Goswami, Y., 2011. Performance analysis of a Rankine-Goswami combined cycle. In Proceedings of the ASME 2011, Washington, DC.

Demirkaya, G., Vasquez Padilla, R., Goswami, D. Y., Stefanakos, E., and Rahman, M. M., 2011. Analysis of a combined power and cooling cycle for low-grade heat sources. International Journal of Energy Research, 35(13):1145–1157.

Eyidogan, M., Canka Kilic, F., Kaya, D., Coban, V., and Cagman, S., 2016. Investigation of Organic Rankine Cycle (ORC) technologies in Turkey from the technical and economic point of view. Renewable and Sustainable Energy Reviews, 58:885–895.

Fazeli, A., Rezvantalab, H., and Kowsary, F., 2011. Thermodynamic analysis and simulation of a new combined power and refrigeration cycle using artificial neural network. Thermal Science, 15(1): 29–41.

Ganesan, V., 2012. Internal Combustion Engines. Tata McGraw-Hill Education Pvt. Ltd, United States, 768p.

Hajime Akimoto., 2016. Atmospheric Reaction Chemistry. Springer, Japan, 449p.

Hardcover, B., 2011. Food Processing Handbook. Wiley and Sons, 826p.

Http://www.lindegas.com/en/products_and_supply/refrigerants/hfo_refrigerants/index.html (Access date: 03 January 2017)

Http://www.volk37.com/alternatives-of-r134a-refrigerant-in-car-ac/ (Access date: 03 January 2017)

Jadhao, J. S., and Thombare, D. G., 2013. Review on Exhaust Gas Heat Recovery for Internal Combustion Engine. International Journal of Engineering and Innovative Technology, 2(12):93–100.

Kanegsberg, B., Handbook for Critical Cleaning: Cleaning Agents and Systems, (2011). CRC Press Inc., United States, 560p.

Kaplowitz, N., Deleve, L. D., 2013. New Drug-Induced Liver Disease. Elsevier Science Publishing Co Inc. 776p.

Karellas, S., and Braimakis, K., 2016. Energy – exergy analysis and economic investigation of a cogeneration and trigeneration ORC – VCC hybrid system utilizing biomass fuel and solar power. Energy Conversion and Management, 107:103–113.

Katsanos, C. O., Hountalas, D. T., and Pariotis, E. G., 2012. Thermodynamic analysis of a Rankine cycle applied on a diesel truck engine using steam and organic medium. Energy Conversion and Management, 60:68–76.

Kim, K. H., and Perez-Blanco, H., 2015. Performance analysis of a combined organic Rankine cycle and vapor compression cycle for power and refrigeration cogeneration. Applied Thermal Engineering, 91:964–974.

Kim, K. H., Shon, Z. H., Nguyen, H. T., and Jeon, E. C., 2011. A review of major chlorofluorocarbons and their halocarbon alternatives in the air. Atmospheric Environment, 45(7):1369–1382.

Kreider, J. F., (2000). Handbook of Heating, Ventilation, and Air Conditioning. CRC Press, 680p.

Li, G., 2016. Organic Rankine cycle performance evaluation and thermoeconomic assessment with various applications part I: Energy and exergy performance evaluation. Renewable and Sustainable Energy Reviews, 53:477–499.

Li, H., Bu, X., Wang, L., Long, Z., and Lian, Y., 2013. Hydrocarbon working fluids for a Rankine cycle powered vapor compression refrigeration system using low-grade thermal energy. Energy and Buildings, 65:167–172.

Macián, V., Serrano, J. R., Dolz, V., and Sánchez, J., 2013. Methodology to design a bottoming Rankine cycle, as a waste energy recovering system in vehicles. Study in a HDD engine. Applied Energy, 104:758–771.

Maunder, W. J., 1992. Stockholm Environment Institute., and World Climate Conference (2nd : 1990 : Geneva, S. (1992), Dictionary of global climate change, Chapman and Hall.

McConnell, R. L., and Abel, D. C., 2015. Environmental geology today. Jones and Bartlett Learning, 824p.

Molés, F., Navarro-Esbrí, J., Peris, B., Mota-Babiloni, A., and Kontomaris, K. (Kostas)., 2015a. Thermodynamic analysis of a combined organic Rankine cycle and vapor compression cycle system activated with low temperature heat sources using low GWP fluids. Applied Thermal Engineering, 87:444–453.

Molés, F., Navarro-Esbrí, J., Peris, B., Mota-Babiloni, A., and Kontomaris, K. (Kostas)., 2015b. Thermodynamic analysis of a combined organic Rankine cycle and vapor compression cycle system activated with low temperature heat sources using low GWP fluids. Applied Thermal Engineering, 87:444–453.

Mota-Babiloni, A., Navarro-Esbrí, J., Barragán, Á., Molés, F., and Peris, B., 2014. Drop-in energy performance evaluation of R1234yf and R1234ze(E) in a vapor compression system as R134a replacements. Applied Thermal Engineering, 71(1):259–265.

Nasir, M. T., and Kim, K. C., 2016. Working fluids selection and parametric optimization of an Organic Rankine Cycle coupled Vapor Compression Cycle (ORC-VCC) for air conditioning using low grade heat. Energy and Buildings, 129:378–395.

Popli, S., Rodgers, P., and Eveloy, V., 2012. Trigeneration scheme for energy efficiency enhancement in a natural gas processing plant through turbine exhaust gas waste heat utilization. Applied Energy, 93:624–636.

Quoilin, S., Declaye, S., Legros, A., Guillaume, L., and Lemort, V., 2012. Working fluid selection and operating maps for Organic Rankine Cycle expansion machines.

Ram Darash Patel, Priti Shukla, S. G., 2013. Thermodynamic Analysis of Combined Power and Cooling Cycle Using Process Heat from a Passout Turbine as a Heating Source. International Journal of Engineering Research and Technology 2(2):1–5.

Rashidi, M. M., Beg, O. a., Parsa, a. B., and Nazari, F., 2011. Analysis and optimization of a transcritical power cycle with regenerator using artificial neural networks and genetic algorithms. Proceedings of the Institution of Mechanical Engineers, Part A: Journal of Power and Energy, 225(6):701–717.

Roy, J. P., Mishra, M. K., and Misra, A., 2010. Parametric optimization and performance analysis of a waste heat recovery system using Organic Rankine Cycle. Energy, 35(12):5049–5062.

Saleh, B., 2016. Parametric and working fluid analysis of a combined organic Rankine-vapor compression refrigeration system activated by low-grade thermal energy. Journal of Advanced Research, 7(5):651–660.

Sarbu, I., 2014. A review on substitution strategy of non-ecological refrigerants from vapour compression-based refrigeration, air-conditioning and heat pump systems. International Journal of Refrigeration, 46:123–141.

Sarr, J. A. R., and Mathieu-Potvin, F., 2016. Increasing thermal efficiency of Rankine cycles by using refrigeration cycles: A theoretical analysis. Energy Conversion and Management, 121:358–379.

Schnubel, M., 2009. Today's Technician: Automotive Heating and Air Conditioning Classroom Manual and Shop Manual. Delmar Cengage Learning, 441p.

Schuster, A., Karellas, S., Kakaras, E., and Spliethoff, H., 2009. Energetic and economic investigation of Organic Rankine Cycle applications. Applied Thermal Engineering, 29(8):1809–1817.

Shu, G., Li, X., Tian, H., Liang, X., Wei, H., and Wang, X., 2014. Alkanes as working fluids for high-temperature exhaust heat recovery of diesel engine using organic Rankine cycle. Applied Energy, 119:204–217.

Shu, G., Yu, G., Tian, H., Wei, H., and Liang, X., 2014. A Multi-Approach Evaluation System (MA-ES) of Organic Rankine Cycles (ORC) used in waste heat utilization. Applied Energy, 132: 325–338.

Smith, J., 2006. The Facts on File Dictionary of Earth Science (Facts on File Science Dictionary). Facts on File, 387p.

Voogt, P. D., 2012. Reviews of Environmental Contamination and Toxicology Volume 208: Perfluorin. Springer, 224p.

Wang, E., Zhang, H., Fan, B., and Wu, Y., 2012. Optimized performances comparison of organic Rankine cycles for low grade waste heat recovery. Journal of Mechanical Science and Technology, 26(8):2301–2312.

Wang, H., Peterson, R., and Herron, T., 2011. Design study of configurations on system COP for a combined ORC (organic Rankine cycle) and VCC (vapor compression cycle). Energy, 36(8): 4809–4820.

Wang, H., Peterson, R., Harada, K., Miller, E., Ingram-Goble, R., Fisher, L., and Ward, C., 2011. Performance of a combined organic Rankine cycle and vapor compression cycle for heat activated cooling. Energy, 36(1):447–458.

Wang, J., Yan, Z., Zhou, E., and Dai, Y., 2013. Parametric analysis and optimization of a Kalina cycle driven by solar energy. Applied Thermal Engineering, 50(1):408–415.

Whitman, B., Johnson, B. 2016. New Refrigeration and Air Conditioning Technology. Delmar Cengage Learning, 1696p.

Yang, M. H., and Yeh, R. H., 2014. Analyzing the optimization of an organic Rankine cycle system for recovering waste heat from a large marine engine containing a cooling water system. Energy Conversion and Management, 88:999–1010.

Yang, M.-H., 2016. Optimizations of the waste heat recovery system for a large marine diesel engine based on transcritical Rankine cycle. Energy, 113:1109-1124.

Yataganbaba, A., Kilicarslan, A., and Kurtbaş, I., 2015. Exergy analysis of R1234yf and R1234ze as R134a replacements in a two evaporator vapour compression refrigeration system. International Journal of Refrigeration, 60:26–37.

Yilmaz, A., 2015. Transcritical organic Rankine vapor compression refrigeration system for intercity bus air-conditioning using engine exhaust heat. Energy, 82:1047–1056.

Yu, G., Shu, G., Tian, H., Wei, H., and Liu, L., 2013. Simulation and thermodynamic analysis of a bottoming Organic Rankine Cycle (ORC) of diesel engine (DE). Energy, 51:281–290.

Yue, C., Han, D., Pu, W., and He, W., 2015. Comparative analysis of a bottoming transcritical ORC and a Kalina cycle for engine exhaust heat recovery. Energy Conversion and Management, 89:764–774.

Yue, C., You, F., and Huang, Y., 2016. Thermal and economic analysis of an energy system of an ORC coupled with vehicle air conditioning. International Journal of Refrigeration, 64:152–167.

Zhang, C., Shu, G., Tian, H., Wei, H., and Liang, X., 2015. Comparative study of alternative ORC-based combined power systems to exploit high temperature waste heat. Energy Conversion and Management, 89:541–554.

Zhang, X., He, M., and Zhang, Y., 2012. A review of research on the Kalina cycle. Renewable and Sustainable Energy Reviews, 16(7):5309–5318.

Zhang, X., Zeng, K., Bai, S., Zhang, Y., And He, M., 2011. Exhaust Recovery of Vehicle Gasoline Engine Based on Organic Rankine Cycle. 2011:04-12.

Zhao, R., Zhuge, W., Zhang, Y., Yin, Y., Chen, Z., and Li, Z., 2014. Parametric study of power turbine for diesel engine waste heat recovery. Applied Thermal Engineering, 67(1–2):308–319.

Zhao, Y., Qi, Z., Chen, J., Xu, B., and He, B., 2012. Experimental analysis of the low-GWP refrigerant R1234yf as a drop-in replacement for R134a in a typical mobile air conditioning system. Proceedings of the Institution of Mechanical Engineers, Part C: Journal of Mechanical Engineering Science, 226(11):2713–2725.

Zhu, S., Deng, K., and Qu, S., 2013. Energy and exergy analyses of a bottoming rankine cycle for engine exhaust heat recovery. Energy, 58:448–457.

Zilio, C., Brown, J. S., Schiochet, G., and Cavallini, A., 2011. The refrigerant R1234yf in air conditioning systems. Energy, 36(10):6110–6120.

CURRICULUM VITAE

Arif Emre AKTAŞ was born on July 07,1988 in Amasya. After completing his education in Kemalpaşa İlköğretim okulu in GHK, and Merzifon Anatolia High School in Merzifon, he enrolled in Çukurova University Automotive Engineering Department in 2009. He had graduated in 2014. In the same year, he had started to Master of Science education in Automotive Engineering Department

APPENDIX

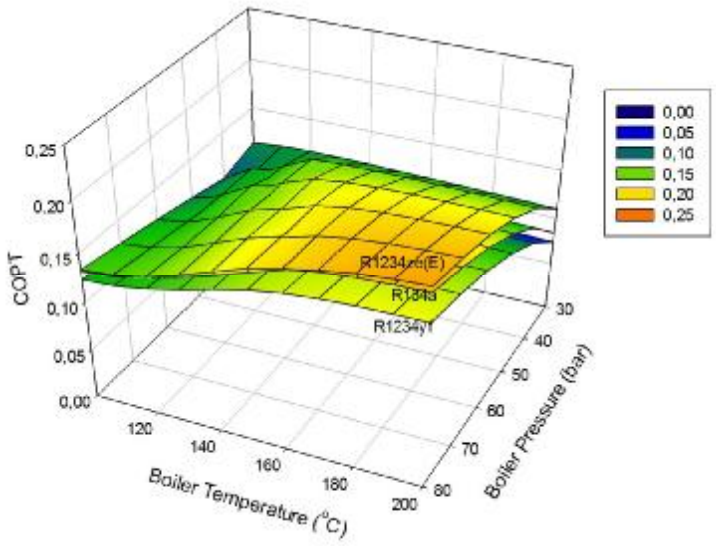

Figure A.1. Variation of COPT with boiler pressure and boiler temperatures at T_{con}:60 °C, T_{eva}:0 °C, $\Delta T_{sub}=\Delta T_{sup}$=1 °C and LV efficiencies

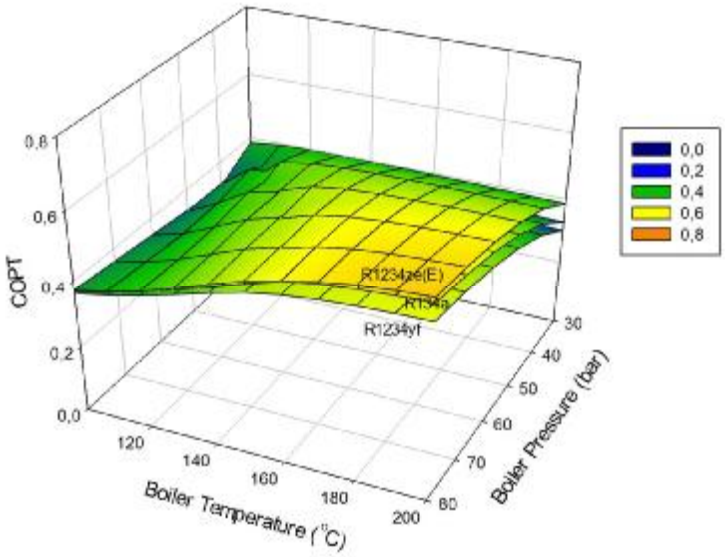

Figure A.2. Variation of COPT with boiler pressure and boiler temperatures at T_{con}:45 °C, T_{eva}:15 °C, $\Delta T_{sub}=\Delta T_{sup}$=1 °C and LV efficiencies

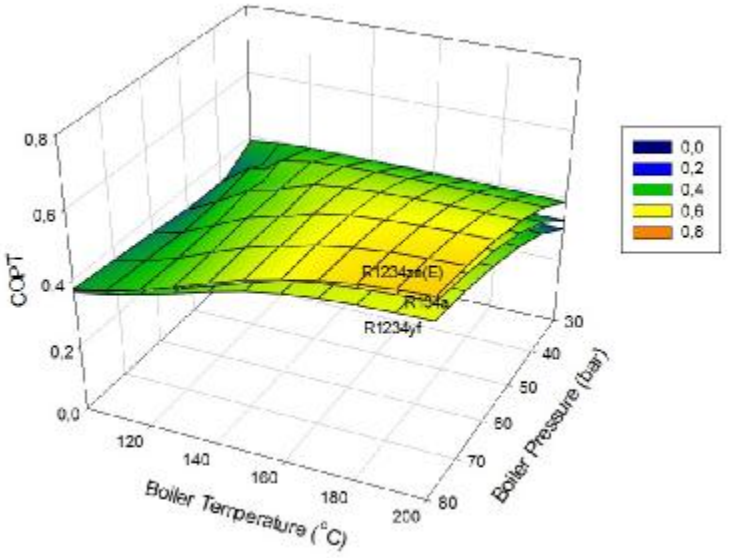

Figure A.3. Variation of COPT with boiler pressure and boiler temperatures at T_{con}:60 °C, T_{eva}:0 °C, $\Delta T_{sub}=\Delta T_{sup}$=5 °C and LV efficiencies

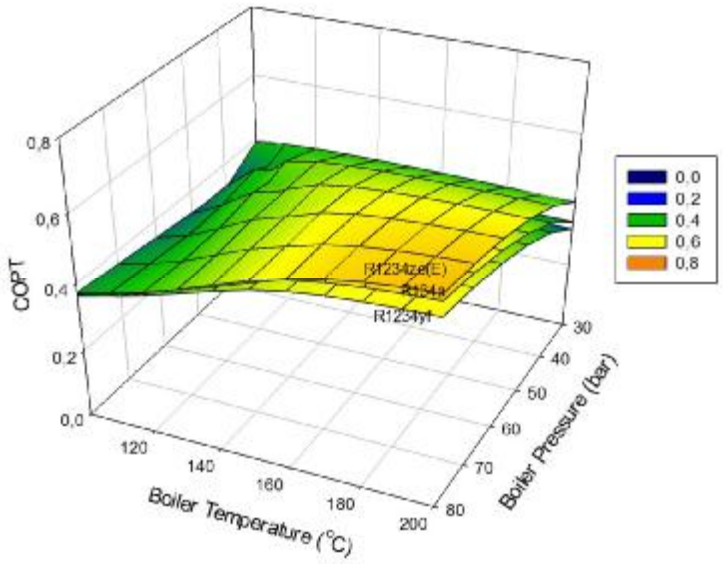

Figure A.4. Variation of COPT with boiler pressure and boiler temperatures at T_{con}:45 °C, T_{eva}:15 °C, $\Delta T_{sub}=\Delta T_{sup}$=5 °C and LV efficiencies

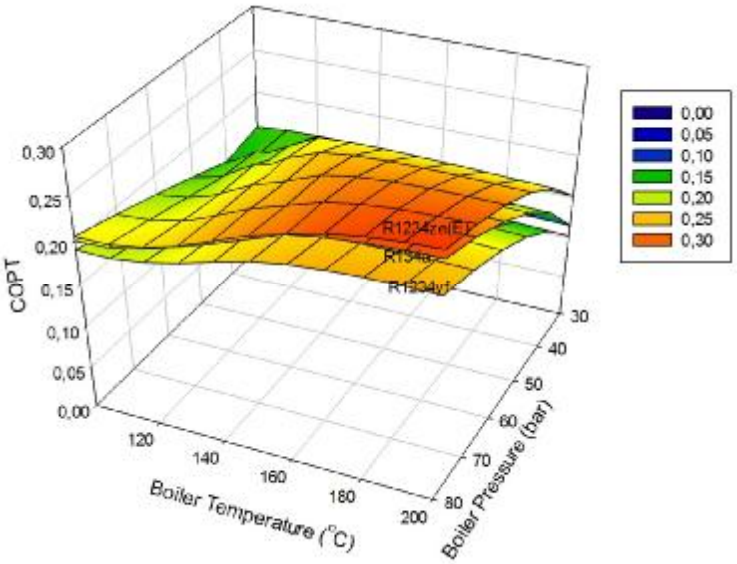

Figure A.5. Variation of COPT with boiler pressure and boiler temperatures at T_{con}:60 °C, T_{eva}:0 °C, $\Delta T_{sub}=\Delta T_{sup}$=1 °C and MV efficiencies

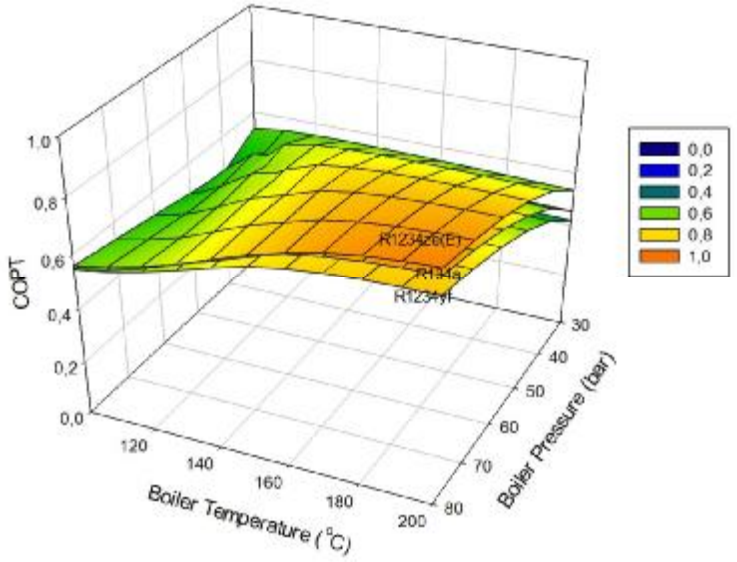

Figure A.6. Variation of COPT with boiler pressure and boiler temperatures at T_{con}:45 °C, T_{eva}:15 °C, $\Delta T_{sub}=\Delta T_{sup}$=1 °C and MV efficiencies

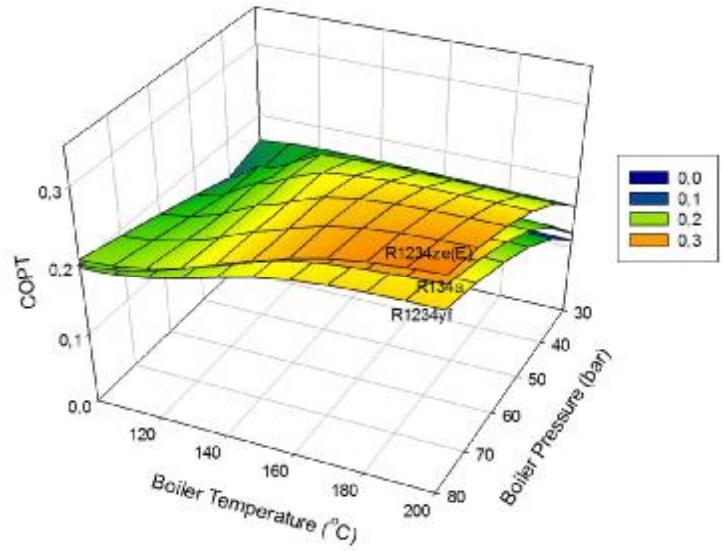

Figure A.7. Variation of COPT with boiler pressure and boiler temperatures at T_{con}:60 °C, T_{eva}:0 °C, $\Delta T_{sub}=\Delta T_{sup}$=5 °C and MV efficiencies

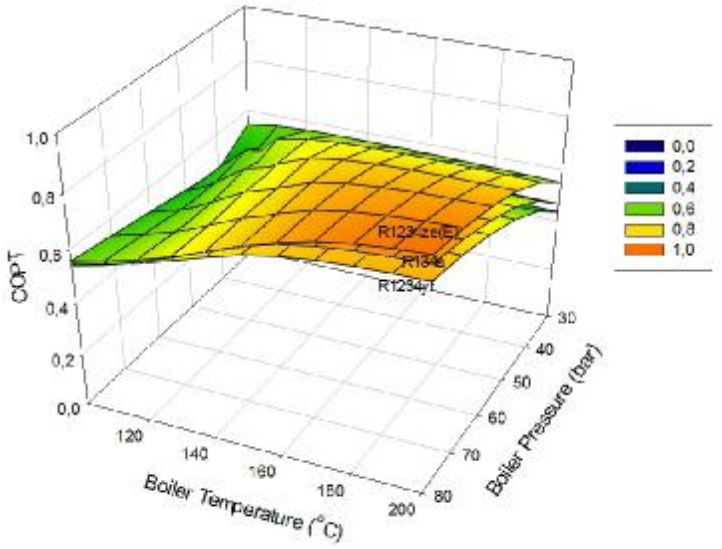

Figure A.8. Variation of COPT with boiler pressure and boiler temperatures at T_{con}:45 °C, T_{eva}:15 °C, $\Delta T_{sub}=\Delta T_{sup}$=5 °C and MV efficiencies

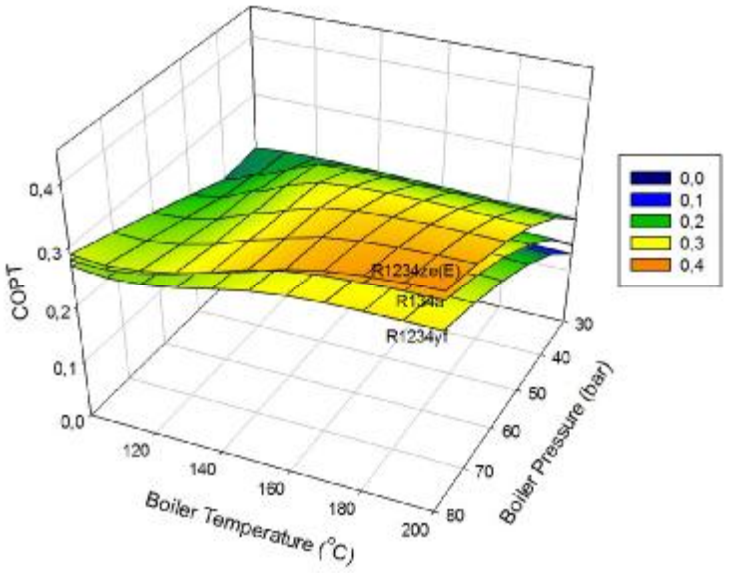

Figure A.9. Variation of COPT with boiler pressure and boiler temperatures at T_{con}:60 °C, T_{eva}:0 °C, $\Delta T_{sub}=\Delta T_{sup}$=1 °C and HV efficiencies

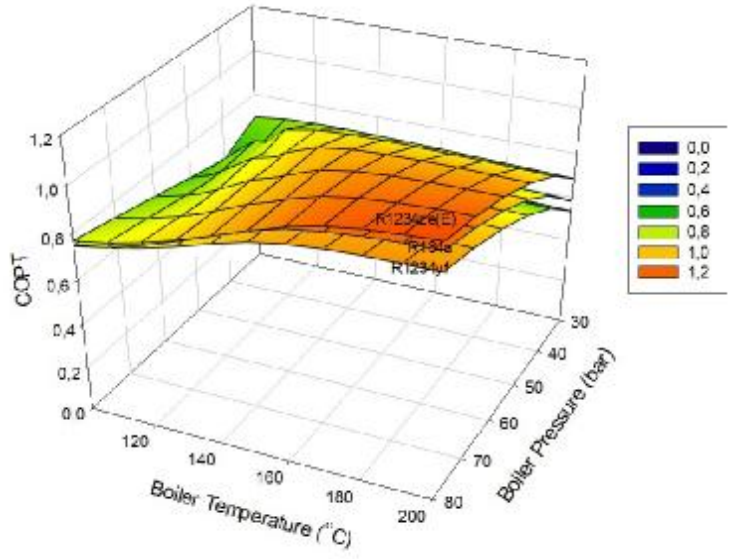

Figure A.10. Variation of COPT with boiler pressure and boiler temperatures at T_{con}:45 °C, T_{eva}:15 °C, $\Delta T_{sub}=\Delta T_{sup}$=1 °C and HV efficiencies

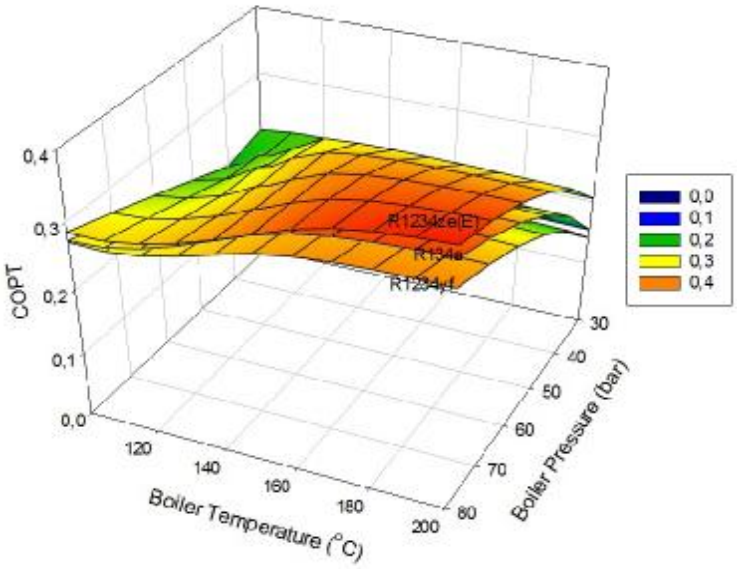

Figure A.11. Variation of COPT with boiler pressure and boiler temperatures at T_{con}:60 °C, T_{eva}:0 °C, $\Delta T_{sub}=\Delta T_{sup}$=5 °C and HV efficiencies

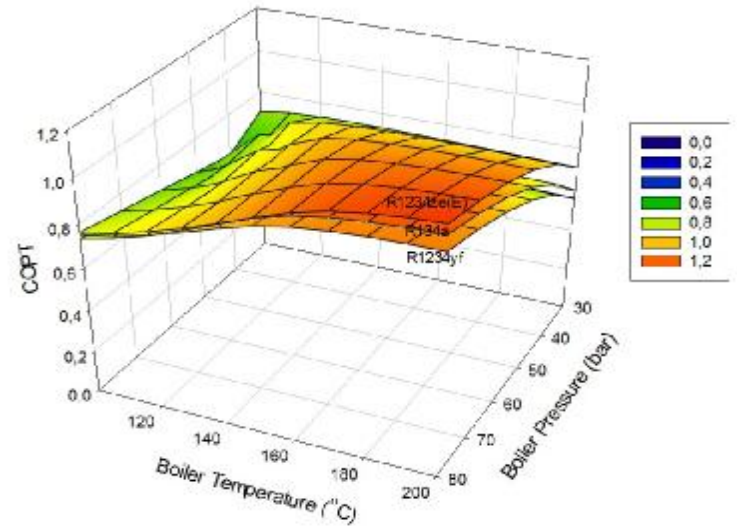

Figure A.12. Variation of COPT with boiler pressure and boiler temperatures at T_{con}:45 °C, T_{eva}:15 °C, $\Delta T_{sub}=\Delta T_{sup}$=5 °C and HV efficiencies

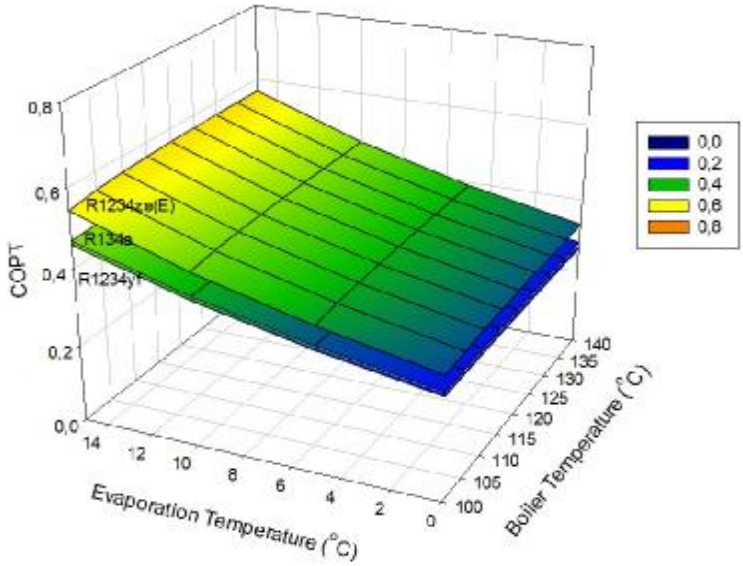

Figure A.13. Variation of COPT with boiler and evaporation temperatures at T_{con}:45 °C, P_{boil}:30 bar, $\Delta T_{sub}=\Delta T_{sup}$=5 °C and MV efficiencies

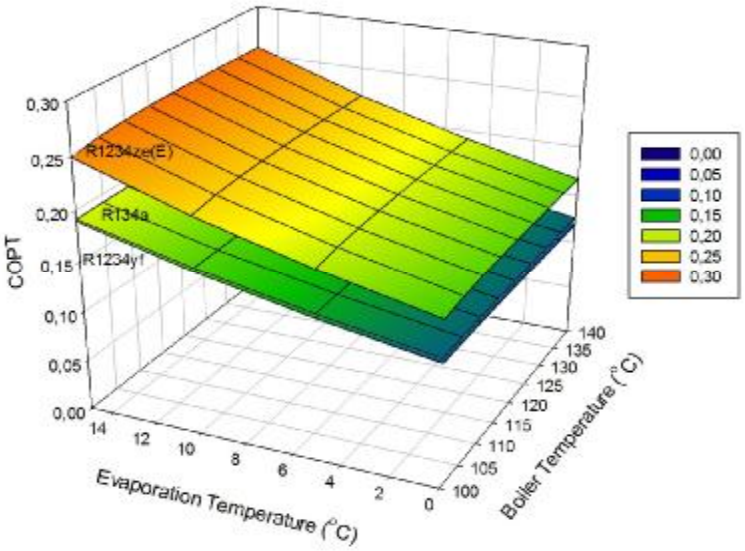

Figure A.14. Variation of COPT with boiler and evaporation temperatures at T_{con}:60 °C, P_{boil}:30 bar, $\Delta T_{sub}=\Delta T_{sup}$=5 °C and MV efficiencies

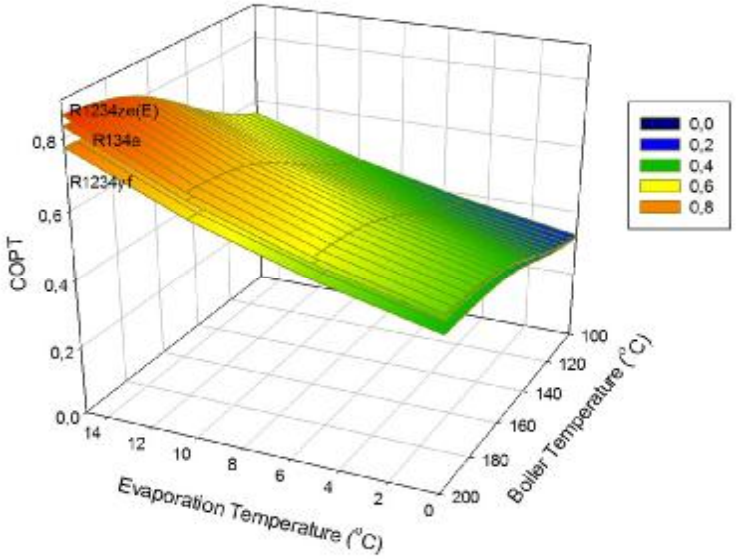

Figure A.15. Variation of COPT with boiler and evaporation temperatures at T_{con}:45 °C, P_{boil}:80 bar, $\Delta T_{sub}=\Delta T_{sup}$=5 °C and MV efficiencies

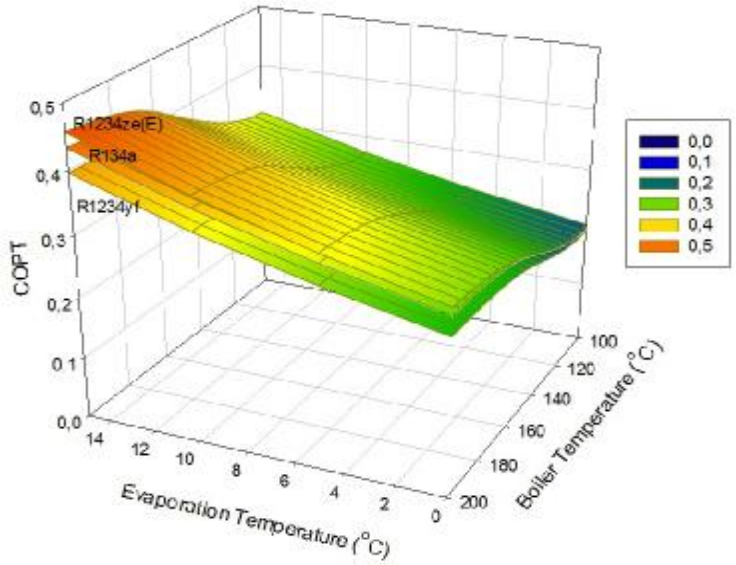

Figure A.16. Variation of COPT with boiler and evaporation temperatures at T_{con}:60 °C, P_{boil}:80 bar, $\Delta T_{sub}=\Delta T_{sup}$=5 °C and MV efficiencies

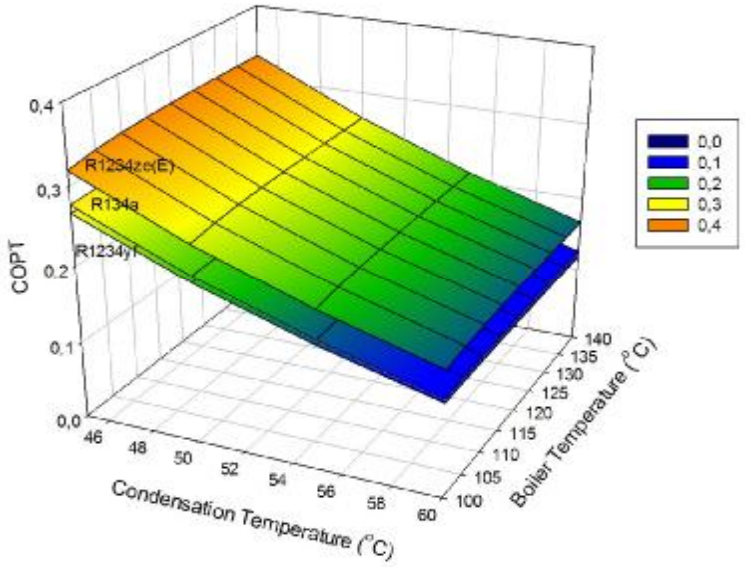

Figure A.17. Variation of COPT with boiler and condensation temperatures at T_{eva}:0 °C, P_{boil}:30 bar, $\Delta T_{sub}=\Delta T_{sup}$=5 °C and MV efficiencies

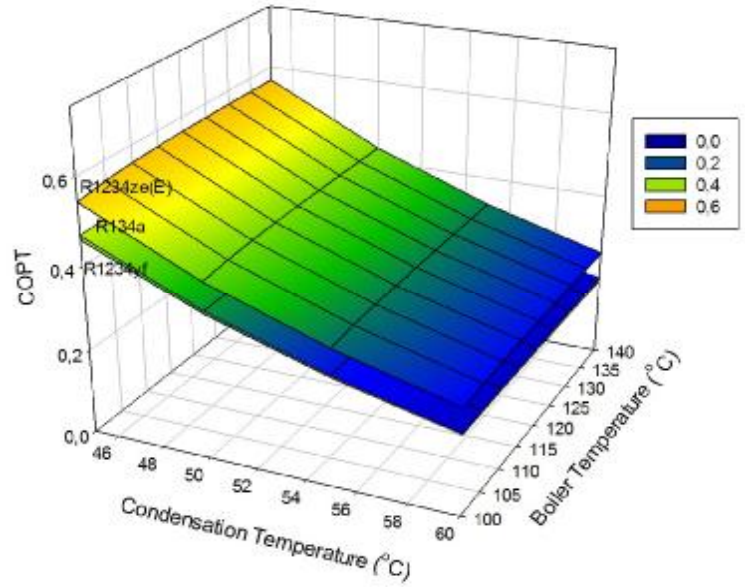

Figure A.18. Variation of COPT with boiler and condensation temperatures at T_{eva}:15 °C, P_{boil}:30 bar, $\Delta T_{sub}=\Delta T_{sup}$=5 °C and MV efficiencies

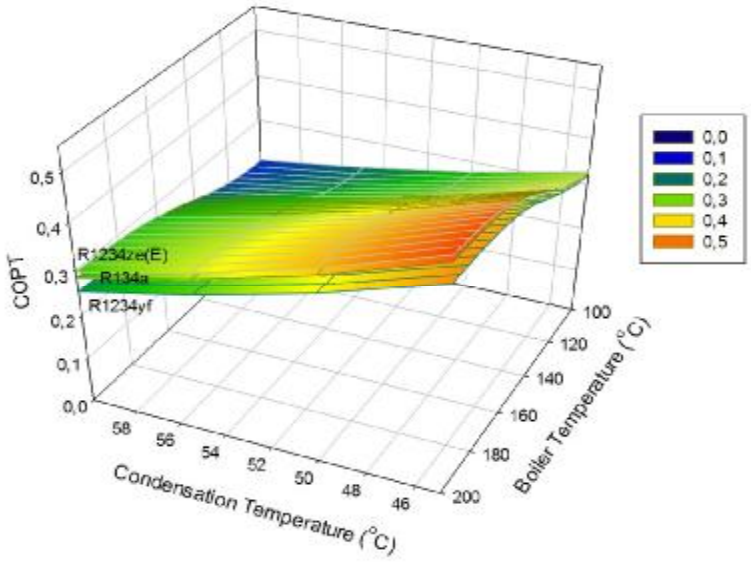

Figure A.19. Variation of COPT with boiler and condensation temperatures at T_{eva}:0 °C, P_{boil}:80 bar, $\Delta T_{sub}=\Delta T_{sup}$=5 °C and MV efficiencies

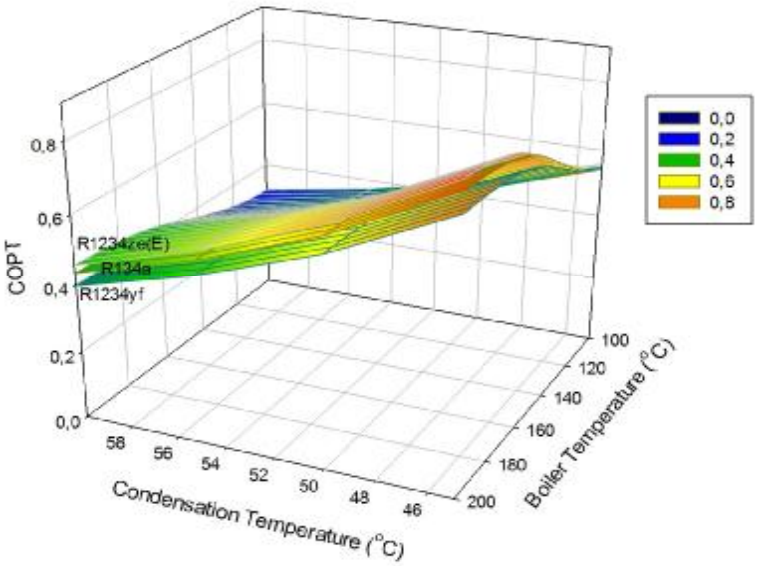

Figure A.20. Variation of COPT with boiler and condensation temperatures at T_{eva}:15 °C, P_{boil}:80 bar, $\Delta T_{sub}=\Delta T_{sup}$=5 °C and MV efficiencies

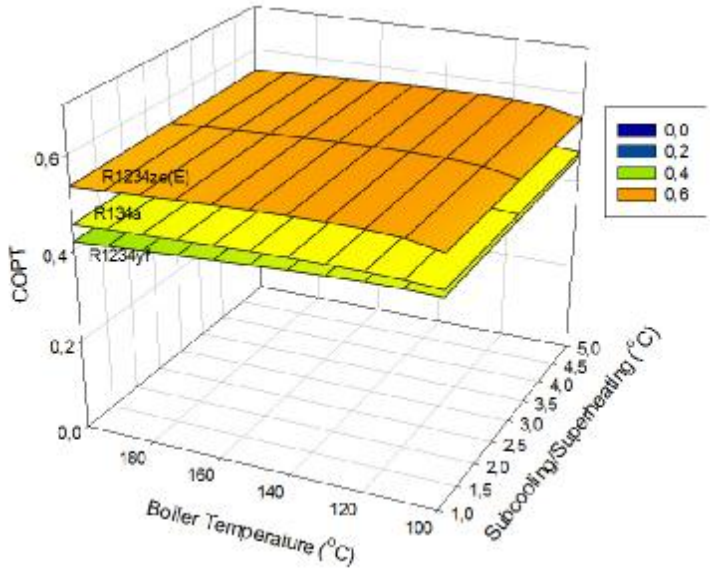

Figure A.21. Variation of COPT with boiler and subcooling/superheating temperatures at P_{boil}:30 bar, T_{eva}:15 °C, T_{con}:45 °C and MV efficiencies

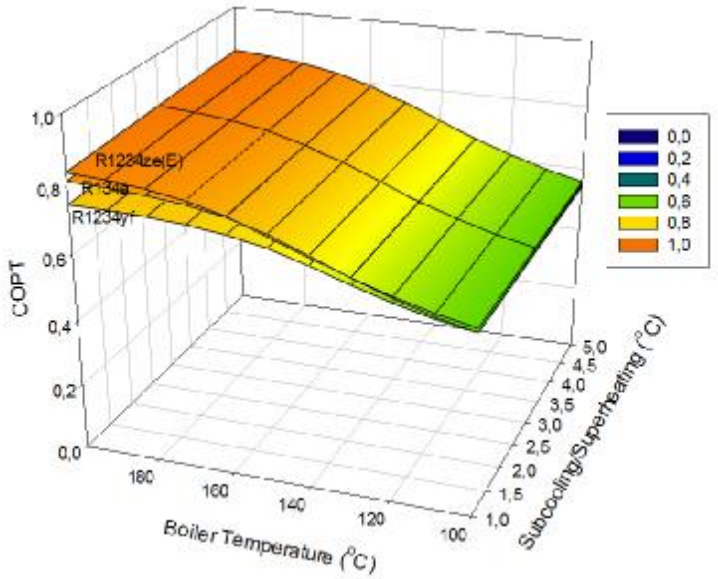

Figure A.22. Variation of COPT with boiler and subcooling/superheating temperatures at P_{boil}:80 bar, T_{eva}:15 °C, T_{con}:45 °C and MV efficiencies

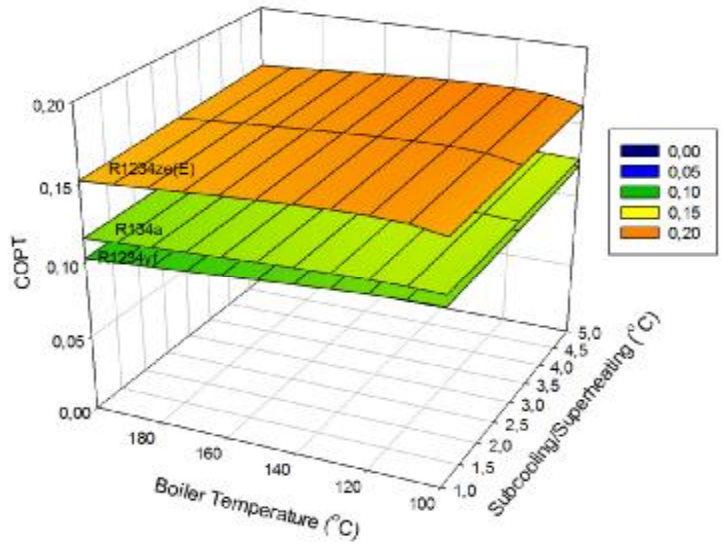

Figure A.23. Variation of COPT with boiler and subcooling/superheating temperatures at P_{boil}:30 bar, T_{eva}:0 °C, T_{con}:60 °C and MV efficiencies

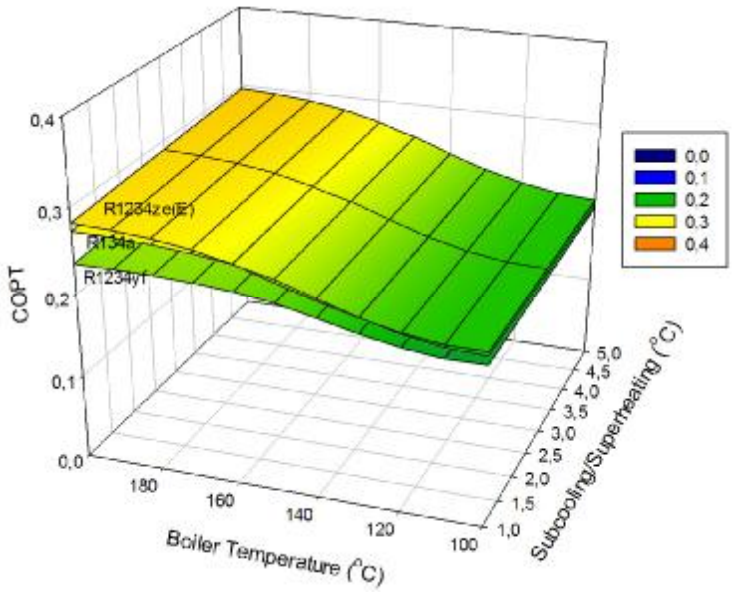

Figure A.24. Variation of COPT with boiler and subcooling/superheating temperatures at P_{boil}:80 bar, T_{eva}:0 °C, and T_{con}:60 °C and MV efficiencies